Impact of chemical reaction on magnetohydrodynamics non-Darcian mixed convective nanofluid flow past over a stretching sheet with non-uniform heat source/sink

Arindam Sarkar[1], Hiranmoy Mondal[*2], Raj Nandkeolyar[1]

[1] Department of Mathematics, National Institute of Technology Jamshedpur, Jamshedpur, 831014, India
Email: arindamjamalpur@gmail.com (+919475486298)
rajnandkeolyar@gmail.com (+917837181319)
[*2]Department of Applied Mathematics, Maulana Abul Kalam Azad University of Technology, West Bengal, Kolkata-700064, India
[*]**Corresponding Author email: hiranmoymondal@yahoo.co.in** (+918617675134)

Abstract

In the current perusal, we have discussed the impacts of free-forced convective heat-mass transportation on magnetohydrodynamic MHD, incompressible, non-Darcy nanofluid flow passing through a porous surface in the presence of an electrical field and a constant magnetic field with chemical reaction. A suitable similarity transformation is being used to non – dimensionalize the system of governing equations along with boundary conditions. The converted system has been solved numerically by operating the Spectral Quasi-linearization method $\left(SQLM\right)$. The effect of various key parameters has been discussed graphically. Velocity seems to be decreasing with the Schmidt number, chemical reaction parameter, Brownian motion parameter, and Hartman number. The Hartman number and the Brinkman number decline the Bejan number in the neighbourhood of the stretching sheet. Nevertheless, far from the stretching sheet, impacts of both Brinkman as well as Hartman number on the Bejan number is negligible. On the other hand, thermal layouts, concentration layouts, and entropy generation are enhanced with the increment in the Hartman number. For the physical interest the coefficients of the skin-friction, heat transfer coefficient, and local Sherwood number also has been determined numerically.

Keywords

Permeable medium, Chemical reaction, Mixed convection, MHD, nanofluid, $SQLM$, non-uniform heat source/sink.

1. Introduction

Nanofluids have unique features that make them potentially beneficial in numerous applications in heat transfer, pharmaceutical process, micro forming, fuel cells, heat exchanger, cancer treatment, polymer and plastic extrusion, glass blowing, cooling and air conditioning and many more. Nanofluid is a combination of nanometer-sized particles with fluid, Choi first introduced it.

Tlili et al. [1] investigated the Darcy Forchheimer Powell-Eyring nanofluid flow in a permeable media with convective boundary conditions and chemical reaction under the impacts of zero mass flux. They solved the governing equations by the Homotopy analysis method. Generation of entropy analysis is also considered in their investigation. Khan et al. [2] studied unsteady flow of a bio-convective Maxwell nanofluid with multiple slip boundary conditions. They used bvp4c-shooting technique. They observed that with the enhance of time relaxation parameter, Sherwood number, Nusselt number, microorganism number, skin friction decline. Ramzan et al. [3] scrutinized the influence of thermal radiation, activation energy on Casson nanofluid flow in the presence of Hall current. They used bvp4c-shooting technique. In addition to in each graphs the consequences of magnetic fields (both inclined and vertical) with fixed angles are portrayed. Nadeem et al. [4] examined a bio-convective unsteady incompressible micropolar nanofluid flow with magnetic field effect. Utilizing shooting method solved non-linear ordinary differential equations numerically. They observed the velocity, microorganism number, thermal energy increased for large value of slip parameters. Mondal et al. [5] studied the impacts of thermophoresis and Brownian motion parameters taking into consideration the convective boundary conditions on power-law (non-Newtonian) fluid. Utilizing the spectral quasi-linearization method, they solved non-linear ordinary differential equations numerically. Furthermore, they observed velocity enhances with mixed convection parameter and the power law index. Khan et al. [6] investigated heat transfer rate of a micropolar fluid in presence of heat generation using Fourier's heat flux model in the heat transfer analysis. He also observed a direct relation between Nusselt number and micropolar parameter while Skin friction demonstrates the opposite behavior with micropolar parameter. Ahmad et al. [7] investigated micropolar nanofluid immerging two distinct nanoparticles in it. They solved the coupled fluid problems by applying bvp4c-shooting technique. In their investigation they observed that generation of entropy enhances with Brinkmann number while Bejan number diminishes.

Khan et al. [8] investigated mass and thermal transport analysis of Maxwell nanofluid Under the influence of thermophoretic and Brownian motion parameters. They observed that the heat transportation rate upsurges for large values of Biot number. Ramzan et al. [9] investigated the effect of magnetic dipole on Oldroyd-B fluid flow. They observed that the velocity and temperature profile decrease with ferromagnetic parameter. Kumar et al. [10] studied the velocity slip impact on nanoscale fluid flow passing through a rotating disk. Under the influence of double stratification and heat generation/absorption, Ahmad et al. [11] investigated steady Maxwell nanofluid three-dimensional flow. Used $bvp4c$ Matlab numerical method. They noticed that the thermal boundary layer increases with the enhancement of the heat generation parameter.

Hall current is a very significant parameter whenever investigating the fluid flow with magnetic effect. Hall current is produced when an electric field acts as a conductor in the appearance of a magnetic field. The effect of Hall current with ion-slip has been investigated by Krishna et al. [12].

They found that with the increment of Hall current velocity profile enhanced all through the field. Furthermore, they also observed that on tony Hall current also the increment of ion slip condition is behind the enhancement of the velocity profile. Khan et al. $[13]$ investigated the hybrid nano-fluid flow comprise of Silicon dioxide and Molybdenum Di-sulphide, they conclude that velocity and temperature show opposing behaviour due to the increment of the suction parameter, velocity is enhanced while temperature deteriorates.

In physics, industrial activity, and chemistry there is a significant impact of magnetic field on nanofluids. A fluid stream in presence of an electric field along with a magnetic field can control stretching – cooling rate. Such implementation has been observed by Vaidya et al. $[14]$, they considered a three-dimensional Jeffery nanofluid over a bidirectional extended lamina, taking zero mass concentration velocity slip. They have noted that Deborah's number clashes with the velocity layout. Ramzan et al. $[15]$ studied the influences of heat generation/absorption and Cattaneo-Christov heat flux on MHD Ethylene glycol based Fe_3O_4 nanofluid in a permeable media. They noticed velocity slip, porosity parameters, and nanoparticles volume fraction decline velocity profile. Khan et al. $[16]$ audited Oldroyd-B nanofluid two-dimensional flow. They observed velocity decreases with an enhancement of relaxation parameter, while for retardation parameter the opposite behavior for velocity profile has been noticed. Pal et al. $[17]$ analyze the heat generation of a micropolar fluid with Ohmic dissipations including the magnetic field effect. Solved converted ODE by Runge-Kutta-Fehlberg technique. Scrutinized that the increment of the Prandtl number reduces the momentum and thermal boundary layer, and observed a strong influence of Soret – Dufour on mass distribution, they are directly related. Rafiq et al. $[18]$ take into account Jeffrey fluid as a base fluid. Lubrication technique, they have applied to solve nonlinear equations. They reported as, in the neighbourhood of the centre, the velocity layout displays parabolic whereas a blended behavior has been noticed in the vicinity of the boundaries, also noticed tapering effect and velocity layout are inversely related. Reddy et al. $[19]$ utilized the Keller box technique to obtain numerical solutions. They have included slips and without slips conditions. They conclude as, velocity layout enhances with G_r and G_c, but the opposite impact from magnetic parameter (M), and permeability parameter (K), they have noticed. Gul et al. $[20]$ have taken into account the laminar and steady stream of Cu/H_2O and $Cu-Al_2O_3/H_2O$. Dominating $ODEs$ has been solved numerically by the $R-K$ order 4^{th} technique. They noted that the magnetic - dipole controlled fluid – stream turbulence. Sarkar et al. $[21]$ scrutinize the impacts of thermal conductivity, thermal radiation, and temperature-dependent viscosity on Powell-Eyring fluid. Moreover, they consider varying Prandtl number. Used recent spectral quasi-linearization technique to solved transformed ordinary differential equations.

The research work carried out by several researchers $([22],[23],[24],[25],[26],\&[27])$ in the relevant area is presented in the Gap analysis (see Table 1). It is observed that the literature lacks a comprehensive study on the flow of incompressible nanofluids with chemical reactions and nonuniform heat generation/absorption impacts combined with non-isothermal temperature and concentration boundary conditions. In this present study, the main motive of the authors is to illustrate a mathematical model containing the steady two-dimensional incompressible and electrically conducting magnetohydrodynamic nanofluid flow over a stretching sheet under the influence of chemical reaction, mixed convection, nonuniform heat generation, viscous dissipation, Ohmic heating, Brownian motion and thermophoresis with non-isothermal temperature and concentration boundary conditions. At first, the governing non-linear coupled partial differential equations $(PDEs)$ have been transformed into a system of non-linear coupled ordinary differential equations $(ODEs)$ utilizing suitable similarity transformation, and then the converted system has been solved numerically by operating the Spectral Quasi-linearization method $(SQLM)$. A concise description of the generation of entropy and the effects of several relevant flow parameters on the rate of generation of entropy and Bejan number are demonstrated significantly.

In this study, the following scientific research questions are answered:

- How is the concentration affected by the chemical reaction parameter, Brownian motion, thermophoresis, solutal buoyancy parameter, Hartman number, and Schmidt number？
- What is the effect of the Prandtl parameters, Brownian motion, thermophoresis, chemical reaction parameter, Hartman number, and Schmidt number on temperature and rate of heat transfer？
- Is there any significant impacts of the Reynolds number, Hartman number, and Brinkman number on the generation of entropy and Bejan number？
- Determine how Brownian motion, Hartman number, thermophoresis diffusion, solutal buoyancy parameter, and Schmidt number influence on skin-friction coefficient, Nusselt number, and Sherwood number.
- How much $SQLM$ is compatible with other traditional methods？

2. Mathematical Formulation

2.1. Flow investigation

Here we scrutinized the free-forced convective heat-mass transportation boundary layer of a steady, incompressible, laminar, magnetohydrodynamics (MHD) nanofluid flow passing through a vertical non-linear expanded non-Darcian porous surface in the presence of a constant electric field effect $\vec{E}=(0,0,-E_0)$ and a uniform magnetic field $\vec{B}=(0,B_0,0)$ with chemical reaction to stabilize the boundary layer flow as demonstrated in Figure 1.

It has been taken into consideration that the flow produced due to elastic sheet. Gauss law for magnetism and Maxwell-Faraday equations are given by $\nabla.\vec{B}=0$ and $\nabla\times\vec{E}=-\frac{\partial B}{\partial t}=0.$ In case of weak magnetic and electric fields adhere to Ohm's law $\vec{J}=\sigma(\vec{E}+\vec{q}\times\vec{B})$, where $\vec{J}$ signifies Joule current, σ denotes permeability of magnetic field and $\vec{q}$ denotes velocity of the fluid. The magnetic field dominating the electric fluid is in this case. The temperature as well as species concentration have a quadratic form. By presuming the fluid resources are unaltered, Boussinesq approximation implemented in momentum equation. Under prior conventions with non-uniform heat source/sink boundary layer leading equations are given by

$$\frac{\partial u}{\partial x}+\frac{\partial v}{\partial y}=0 \tag{1}$$

$$u\frac{\partial u}{\partial x}+v\frac{\partial u}{\partial y}=\nu\frac{\partial^2 u}{\partial y^2}+\frac{\sigma}{\rho}\left(E_0B_0-B_0^2u\right)-\frac{\nu}{\kappa}u-\frac{c_b}{\sqrt{\kappa}}u^2+g\beta_T\left(T-T_\infty\right)+g\beta_C\left(C-C_\infty\right) \tag{2}$$

Where (u,v) denotes velocity along respective co-ordinate axes x and y, g demonstrate the gravitational acceleration, β_T represents the thermal expansion coefficient, ν indicates kinematic viscosity, ρ signifies the fluid density, T_w stands for wall-temperature, T_∞ denote ambient temperature and T signifies the temperature of the fluid. κ signifies the porous medium permeability, μ represents the dynamic viscosity, in the transverse direction E_0, B_0 signifies the strength of electric and magnetic fields respectively, β_C indicates volumetric coefficients of mass expansion, dimensionless quantity c_b denotes the coefficient of drag force, and electrically conductivity of the fluid denoted by σ. The empirical constant, in the second-order resistance, denoted by $F=\frac{c_b}{\sqrt{\kappa}}$, known as Darcy-Forchheimer number. By substituting $F=0$, Equation 2 becomes Darcy's law. $\frac{\nu}{\kappa}u$ signifies the first-order Darcy and $\frac{c_b}{\sqrt{\kappa}}u^2$ represent second-order inertia resistance due to porosity.

The relevant boundary conditions on velocity are as follows

$u=u_w\left(x\right)=cx, v=0$ at $y=0$,

$$u\rightarrow 0, \text{ as } y\rightarrow\infty \tag{3}$$

Where $u_w\left(x\right)$ is the stretching lamina velocity, c is a constant. To convert the leading momentum Equation 2, the similarity variables take the expressions as follows

$$u=cxf'\left(\eta\right), v=-\sqrt{c\nu}\,f\left(\eta\right), \eta=\sqrt{\frac{c}{\nu}}y. \tag{4}$$

Here $\eta, f\left(\eta\right)$ stands for the non-dimensional similarity space variable and velocity function respectively. Utilizing Equation 4, Equation 2 transformed to a third order non-dimensional ODE as

$$f'''+ff''+Ha^2\left(E_1-f'\right)-f'^2-k_1f'-F^*f'^2+\lambda\theta+\delta H=0 \tag{5}$$

Where $Ha^2=\frac{\sigma B_0^2}{\rho c}$ represents the magnetic parameter, $E_1=\frac{E_0}{B_0cx}$ signify the electric field parameter, $k_1=\frac{\nu}{\kappa c}$ denotes the porous parameter, $F^*=\frac{c_bx}{\sqrt{\kappa}}$ stands for the inertia coefficient, $\lambda=\frac{Gr_x}{\mathrm{Re}_x^2}$ indicates the thermal buoyancy parameter, $\delta=\frac{Gr_c}{\mathrm{Re}_x^2}$ represents the concentration buoyancy parameter, $Gr_x=\frac{g\beta_T\left(T_w-T_\infty\right)}{\nu^2}$, $Gr_c=\frac{g\beta_C\left(C_w-C_\infty\right)}{\nu^2}$ denotes the thermal Grashof number and solutal Grashof number orderly.

Utilizing Equation 4 in Equation 3, converted boundary conditions as follows

$f(\eta)=0, f'(\eta)=1$ at $\eta=0$,

$$f'(\eta)=0 \text{ as } \eta\to\infty. \tag{6}$$

For the physical curiosity the skin friction coefficient C_f, is given by

$$C_f=\frac{\tau_w}{\left(\frac{\rho u_w^2}{2}\right)}, \tag{7}$$

Where, τ_w, wall shear stress is given by

$$\tau_w=\mu\left(\frac{\partial u}{\partial y}\right)_{y=0} \tag{8}$$

The dimensionless form of Equations 7 and 8, utilizing Equation 4 as

$$C_f \operatorname{Re}_x^{\frac{1}{2}}=2f''(0) \tag{9}$$

$\operatorname{Re}_x=\frac{u_w x}{\nu}$ stands for the local Reynolds number.

2.2. Energy conversion on account of similarity transformation

The heat transportation equation in the presence of non-constant heat generation/absorption is given by

$$u\frac{\partial T}{\partial x}+v\frac{\partial T}{\partial y}=\frac{\kappa_f}{\rho c_p}\frac{\partial^2 T}{\partial y^2}+\frac{\mu}{\rho c_p}\left(\frac{\partial u}{\partial y}\right)^2+\frac{\sigma}{\rho c_p}\left(uB_0-E_0\right)^2+\frac{1}{\rho c_p}q'''+\tau\left[D_B\frac{\partial T}{\partial y}\frac{\partial C}{\partial y}+\frac{D_T}{T_\infty}\left(\frac{\partial T}{\partial y}\right)^2\right] \tag{10}$$

Where c_p indicates the specific heat, D_T and D_B stands for the thermophoretic and diffusion coefficient of Brownian, κ_f signifies the thermal conductivity, τ denotes fraction of heat capacity of nanoparticles to the base fluid, and the free stream temperature is given by T_∞. $\frac{\mu}{\rho c_p}\left(\frac{\partial u}{\partial y}\right)^2$ signifies viscous dissipation for unit area and $\frac{\sigma}{\rho c_p}\left(uB_0-E_0\right)^2$ signifies Ohmic dissipation or Joule heating. The electric, as well as magnetic fields, transformed electric or magnetic energy into thermal energy. The non-constant wall temperature of the expanded lamina represented by $T_w(x)$, $\left(T_w(x)>T_\infty\right)$. $T_w(x)$ varies with x, distance from the expanded lamina. Assuming non-isothermal flows i.e., non-constant temperature $T_w(x)$, to solve Equation 10, the boundary conditions are given by

$T = T_w(x) = T_\infty + ax^2$ at $y = 0$,

$T \to T_\infty$ as $y \to \infty$ (11)

Where, a stands for thermal distribution parameter on the expanded lamina. The non-constant heat generation/absorption along the thermal boundary layer is manifested by q''' and given by

$$q''' = \frac{\kappa_f u_w(x)}{x\nu}(T_w - T_\infty)\left[A^* e^{-\eta} + B^*\theta\right], \tag{12}$$

Where space coefficients and heat source/sink denoted by A^* and B^* orderly. Here we consider that $A^* > 0, B^* > 0$ and $A^* < 0, B^* < 0$ indicate internal heat generation and internal heat absorption orderly. Dimensionless temperature variable $\theta(\eta)$ given by

$$\theta = \frac{T - T_\infty}{T_w - T_\infty} \tag{13}$$

Substituting Equations 12 and 13 in Equation 10 we acquire a transformed non-dimensional ODE of order two as

$$\theta'' - \Pr\left(2f'\theta - f\theta'\right) + Ha^2 E_c \Pr\left(E_1 - f'\right)^2 + \Pr E_c f''^2 + \left(A^* e^{-\eta} + B^*\theta\right) + \Pr\left(Nb\theta' H' + Nt\theta'^2\right) \tag{14}$$

Where $\Pr = \frac{\mu c_p}{\kappa_f}$ indicates Prandtl number, Eckert number is denoted by E_c and defined as $E_c = \frac{c^2}{ac_p}$, $Nb = \frac{\tau D_B\left(C_w - C_\infty\right)}{\nu}$ symbolizes the Brownian movement parameter, $Nt = \frac{\tau D_T\left(T_w - T_\infty\right)}{\nu T_\infty}$ materialize the thermophoresis parameter.

The transformed boundary conditions (11) are given by

$\theta(\eta) = 1$ at $\eta = 0$,

$\theta(\eta) = 0$ as $\eta \to \infty$ (15)

Nu_x indicates the local Nusselt number and characterized as

$$Nu_x = \frac{xq_w}{\kappa_f\left(T_w - T_\infty\right)}, \tag{16}$$

The wall heat flux, i.e., q_w is given by

$$q_w = -\kappa_f \left(\frac{\partial T}{\partial y} \right)_{y=0} \tag{17}$$

By utilizing Equations 4 and 13 we acquire the dimensionless form of Equation 16 and 17 as

$$\frac{Nu_x}{\mathrm{Re}_x^{\frac{1}{2}}} = -\theta'(0) \tag{18}$$

2.3. Equation of mass transferred on account of similarity transformation

The Concentration equation is manifested as below

$$u\frac{\partial C}{\partial x} + v\frac{\partial C}{\partial y} = D_m \frac{\partial^2 C}{\partial y^2} + \frac{D_T}{T_\infty}\frac{\partial^2 T}{\partial y^2} - R^*\left(C_w - C_\infty\right) \tag{19}$$

Where D_m indicates the mass diffusivity, $C_w, C_\infty \left(C_w > C_\infty\right)$ signifies concentration at the wall and the ambient uniform concentration respectively.

Assuming non-isothermal flows, i.e., non-constant concentration $C_w(x)$, to solve Equation 19, the boundary conditions are as follows

$$C = C_w(x) = C_\infty + bx^2 \text{ at } y = 0,$$

$$C \to C_\infty \text{ as } y \to \infty, \tag{20}$$

Where, b stands for concentration distribution parameter on the expanded lamina. We illustrate the concentration variable $H(\eta)$ in non-dimensional form as

$$H(\eta) = \frac{C - C_\infty}{C_w - C_\infty} \tag{21}$$

Substituting Equations 4 and 21 in Equation 19 we acquire a converted non-dimensional ODE of order two as

$$H'' + \frac{Nt}{Nb}\theta'' - ScR_1 H + Sc\left(fH' - 2f'H\right) = 0 \tag{22}$$

Where $Sc = \frac{\nu}{D_m}$ indicates Schmidt number. It refers to the fraction of the hydrodynamic boundary layer to mass transfer boundary layer, $R_1 = \frac{R^*}{c}$ symbolize the chemical reaction parameter. By applying (4) and (21), the boundary conditions (20) become

$$H(\eta) = 1 \text{ at } \eta = 0,$$

$$H(\eta) = 0 \text{ as } \eta \to \infty, \tag{23}$$

To calculate the fraction of convective rate of mass transportation from the wall to the rate of diffusion, the dimensionless local Sherwood number, i.e., Sh_x is defined as

$$Sh_x = \frac{xq_m}{D_m\left(C_w - C_\infty\right)} \tag{24}$$

The mass transfer from the lamina, i.e., q_m is given by

$$q_m = -D_m\left(\frac{\partial C}{\partial y}\right)_{y=0} \tag{25}$$

Where molecular diffusivity indicated by D_m.

By utilizing Equations 4 and 21 we acquire the dimensionless form of Equations 24 and 25 as

$$\frac{Sh_x}{\mathrm{Re}_x^{\frac{1}{2}}} = -H'(0) \tag{26}$$

3. Entropy generation analysis

Convective heat transfer or convection is an analysis of the heat transfer due to the movement of the fluid. To increase the thermodynamic proficiency of the system, related to industrial equipment as an example heat exchanger, the fundamental purpose is to enhance thermal contact as well as to reduce power throughout pumping. To diminish the waste of the attainable energy of the system, the generation of entropy, a coherent thermodynamic process has been introduced. Nowadays, the execution of nanofluids in medical and engineering backgrounds is increased substantially, as an end result, it quickens the research to observe the effect of nanoparticles on the generation of entropy. In the current perusal, the generation of entropy of a viscoelastic nanofluid is the most important consideration. In 1996, Bejan first introduced volumetric entropy generation, based on the thermodynamics second law, for two-dimensional $(2D)$ motion in cartesian coordinates as

$$S'''_{gen} = \underbrace{\frac{\kappa_f}{T_\infty^2}\left(\frac{\partial T}{\partial y}\right)^2}_{S_{th}} + \underbrace{\frac{\sigma B_0^2}{T_\infty}u^2}_{S_m} + \underbrace{\frac{RD}{C_\infty}\left(\frac{\partial C}{\partial y}\right)^2 + \frac{RD}{T_\infty}\left(\frac{\partial T}{\partial y}\frac{\partial C}{\partial y}\right)}_{S_{dif}} \tag{27}$$

and S'''_0, the characteristic entropy rate as

$$S'''_0 = \frac{\kappa_f\left(T_w - T_\infty\right)^2}{T_\infty^2 x^2} \tag{28}$$

Equation 27 demonstrates the three components because of the generation of entropy. The first component term S_{th} indicates generation of entropy due to the heat transfer, the second irreversibility term S_m represents irreversibility on account of magnetic field strength and the third term S_{dif} describes irreversibility in the sake of mass transfer/diffusion effect. Utilizing above three terms, Equation 27 can be recast as

$$S'''_{gen} = S_{th} + S_m + S_{dif} \tag{29}$$

N_G, entropy generation number defined as the ratio of the local entropy rate $\left(S'''_{gen}\right)$ to the characteristic entropy generation rate $\left(S'''_0\right)$, i.e.,

$$N_G = \frac{S'''_{gen}}{S'''_0}$$

Non-dimensional form of entropy generation number N_G is given by

$$N_G(\eta) = \frac{S'''_{gen}}{S'''_0} = \mathrm{Re}\,\theta'^2 + \mathrm{Re}\,Ha^2 \frac{Br}{\chi} f'^2 + \mathrm{Re}\Sigma\left(\frac{\Omega}{\chi}\right)\theta' H' + \mathrm{Re}\Sigma\left(\frac{\Omega}{\chi}\right)^2 H'^2 \tag{30}$$

Where Br represents dimensionless Brinkman number related to heat conduction, Ω and χ stands for concentration and temperature associated parameters, while Σ represents a constant parameter as

$$\mathrm{Re} = \frac{u_w(x)x}{\nu}, Br = \frac{\mu u_w^2(x)}{\kappa_f \Delta T}, \Delta T = T_w - T_\infty, \chi = \frac{\Delta T}{T_\infty}, \Sigma = \frac{RDC_\infty}{\kappa_f}, \Delta C = C_w - C_\infty, \Omega = \frac{\Delta C}{C_\infty} \tag{31}$$

Equation 30 can be recast as the sum up of irreversibility originated from heat transportation, i.e., N_1 and the irreversibility on account of both magnetic field and diffusive, i.e., N_2 as

$$N_G = \underset{N_1}{S_{th}} + \underbrace{S_m + S_{dif}}_{N_2},$$

Where $N_1 = S_{th} = \mathrm{Re}\,\theta'^2(\eta)$ and

$$N_2 = S_m + S_{dif} = \mathrm{Re}\,Ha^2 \frac{Br}{\chi} f'^2 + \mathrm{Re}\Sigma\left(\frac{\Omega}{\chi}\right)\theta' H' + \mathrm{Re}\Sigma\left(\frac{\Omega}{\chi}\right)^2 H'^2 \tag{32}$$

To investigate that the generation of entropy will be governed by irreversibility in the sake of heat transfer, Be, Bejan number exhibited as a ratio of entropy caused by heat transfer to the total entropy as;

$$Be = \frac{N_1}{N_G} = \frac{N_1}{N_1 + N_2} = \frac{1}{1+\phi} \tag{33}$$

Where $\phi = \frac{N_2}{N_1}$ stands for the fraction of irreversibility. Generation of entropy is governed by several terms on account of ϕ. Irreversibility caused by heat transfer dominates generation of entropy in the case of $\phi \in [0,1)$. An effect of magnetic and diffusive irreversibility lead generation of entropy in case of $\phi > 1$. In the case of $\phi = 1$, the sequel from the above mentioned three terms of generation of entropy becomes similar. $[0,1]$, represents the range of the Bejan number.

Irreversibility is dominated by the heat transportation when the Bejan number attains its maximum value, i.e., $Be=1,$ on the other hand irreversibility is ruled by both magnetic field as well as diffusion at $Be=0,$ the minimal value of Bejan number. The significance of heat transfer and combined effect of diffusion and magnetic field become equivalent at $Be=0.5.$

4. Numerical solution utilizing the Spectral quasi-linearisation technique

The system of three dimensionless non-linear $ODEs$ $5, 14,$ and 22 along with the boundary constraints $6,$ $15,$ and 23 respectively, has been solved numerically to an excellence accuracy applying $SQLM$. Richard Bellman and Robert Kalaba improved the Newton-Raphson method to QLM (quasi linearization method) before the last fifty years $(1965).$ QLM generally utilize to linearize the non-linear terms associated with the flow governing equations by the help of Taylor series approximation, assuming infinitesimal difference between $(r+1)^{th}$ and r^{th} iteration. This numerical procedure is very operative because of its accuracy and fast convergency. The non-linear components in the above-said $ODEs,$ will be transformed into a recursive sequence with linear terms. Initially, for Equations $3,$ $14,$ and $22,$ we have to define functions $F,$ $\bar{\theta},$ and $\bar{H}$ orderly, as

$$F = f''' + ff'' + Ha^2\left(E_1 - f'\right) - f'^2 - k_1 f' - F^* f'^2 + \lambda\theta + \delta H \tag{34}$$

$$\bar{\theta} = \theta'' - \Pr\left(2f'\theta - f\theta'\right) + Ha^2 E_c \Pr\left(E_1 - f'\right)^2 + \Pr E_c f''^2 + \left(A^* e^{-\eta} + B^*\theta\right) + \Pr\left(Nb\theta' H' + Nt\theta'^2\right) \tag{35}$$

$$\bar{H} = NbH'' + Nt\theta'' - NbScR_1 H + NbSc\left(fH' - 2f'H\right) \tag{36}$$

Applying quasilinearization method on the Equations $5,$ $14,$ and $22,$ generates the iteration as follows:

$$a_{0,r} f'''_{r+1} + a_{1,r} f''_{r+1} + a_{2,r} f'_{r+1} + a_{3,r} f_{r+1} + a_{4,r}\theta_{r+1} + a_{5,r} H_{r+1} = R_F, \tag{37}$$

$$b_{0,r}\theta''_{r+1} + b_{1,r}\theta'_{r+1} + b_{2,r}\theta_{r+1} + b_{3,r} f''_{r+1} + b_{4,r} f'_{r+1} + b_{5,r} f_{r+1} + b_{6,r} H'_{r+1} = R_{\bar{\theta}}, \tag{38}$$

$$c_{0,r} H''_{r+1} + c_{1,r} H'_{r+1} + c_{2,r} H_{r+1} + c_{3,r} f'_{r+1} + c_{4,r} f_{r+1} + c_{5,r}\theta''_{r+1} = R_{\bar{H}} \tag{39}$$

Based on the boundary conditions:

$$f_{r+1}(0)=0,\ f'_{r+1}(0)=1,\ f'_{r+1}(\infty)\to 0,$$

$$\theta_{r+1}(0)=1, \theta_{r+1}(\infty)\to 0,$$

$$H_{r+1}(0)=1, H_{r+1}(\infty)\to 0. \tag{40}$$

The coefficients in Equations $37-39$ are given as:

$$a_{0,r}=1, a_{1,r}=f_r, a_{2,r}=-Ha^2-2f'_r-k_1-F^*\left(2f'_r\right), a_{3,r}=f''_r, a_{4,r}=\lambda, a_{5,r}=\delta,$$

$$b_{0,r}=1, b_{1,r}=\Pr f_r+\Pr NbH_r'+2\Pr Nt\theta_r', b_{2,r}=-2\Pr f_r'+B^*, b_{3,r}=2\Pr E_c f_r''$$

$$b_{4,r}=-2\Pr\theta_r-2Ha^2E_c\Pr\left(E_1-f_r'\right), b_{5,r}=\Pr\theta_r', b_{6,r}=\Pr Nb\theta_r'$$

$$c_{0,r}=Nb, c_{1,r}=NbScf_r, c_{2,r}=-NbScR_1-2NbScf_r', c_{3,r}=-2NbScH_r, c_{4,r}=NbScH_r', c_{5,r}=Nt. \tag{41}$$

The initial guess satisfying the boundary conditions are to be chosen as follows:

$$f_0(\eta)=1-e^{-\eta}, \theta_0(\eta)=e^{-\eta}, H_0(\eta)=e^{-\eta} \tag{42}$$

The characteristic domain $\left[0, L_x\right]$ converted to the standard interval $\left[-1,1\right]$ by the transformation $\eta=\dfrac{L_x\left(x+1\right)}{2}$. The Gauss-Lobatto collocation points

$$x_i=\cos\left(\frac{\pi i}{N}\right), i=0(1)N,\ \ x_i\in\left[-1,1\right] \tag{43}$$

are considered to interpolate the unknown functions. Here N is the number of collocation points.

The elementary notion of the Spectral-collocation method is to assume the derivatives of unknown variables at the collocation nodes by constructing a differentiation matrix $[D]$ in the form of matrix-vector product. As the domain of $[D]$ matrix is $\left[-1,1\right]$, we scale by considering $D1=\dfrac{2D}{L_x}$ for the characteristic domain $\left[0, L_x\right]$ as

$$\frac{dG_r}{d\eta}(\eta)=\sum_{k=0}^{N}D_{jk}g\left(\eta_k\right)=DG_m,\ \ j=0(1)N, \tag{44}$$

Where $G=\left\{g\left(\eta_0\right), g\left(\eta_1\right), g\left(\eta_2\right)g\left(\eta_3\right), \ldots\ldots\ldots\ldots g\left(\eta_N\right)\right\}^T$ is the vector function at the collocation points. The higher order differentiation can be traced as:

$$G_r^{(q)}=D^qG_r \tag{45}$$

Thence, Equations $37-39$ are given as:

$$\begin{aligned}
&A_{11}f_{r+1}+A_{12}\theta_{r+1}+A_{13}H_{r+1}=R_F,\\
&A_{21}f_{r+1}+A_{22}\theta_{r+1}+A_{23}H_{r+1}=R_{\overline{\theta}},\\
&A_{31}f_{r+1}+A_{32}\theta_{r+1}+A_{33}H_{r+1}=R_{\overline{H}}.
\end{aligned} \tag{46}$$

$$A_{11} = diag\left(a_{0,r}\right)D^3 + diag\left(a_{1,r}\right)D^2 + diag\left(a_{2,r}\right)D + diag\left(a_{3,r}\right)I,$$
$$A_{12} = diag\left(a_{4,r}\right)I,$$
$$A_{13} = diag\left(a_{5,r}\right)I,$$

$$A_{21} = diag\left(b_{3,r}\right)D^2 + diag\left(b_{4,r}\right)D + diag\left(b_{5,r}\right)I,$$
$$A_{22} = diag\left(b_{0,r}\right)D^2 + diag\left(b_{1,r}\right)D + diag\left(b_{2,r}\right)I,$$
$$A_{23} = diag\left(a_{6,r}\right)D,$$

$$A_{31} = diag\left(c_{3,r}\right)D^2 + diag\left(c_{4,r}\right)D,$$
$$A_{32} = diag\left(c_{5,r}\right)D^2,$$
$$A_{33} = diag\left(c_{0,r}\right)D^2 + diag\left(c_{1,r}\right)D.$$

In matrix form, this can be written as

$$\begin{bmatrix} A_{11} & A_{12} & A_{13} \\ A_{21} & A_{22} & A_{23} \\ A_{31} & A_{32} & A_{33} \end{bmatrix} \begin{bmatrix} F_{r+1} \\ \bar{\theta}_{r+1} \\ \bar{H}_{r+1} \end{bmatrix} = \begin{bmatrix} R_F \\ R_{\bar{\theta}} \\ R_{\bar{H}} \end{bmatrix}$$

5. Result and discussions

The perusal imparts an impact of the non-dimensional parameters on generation of entropy and Bejan number take into account a MHD, steady $2D$ viscoelastic, nanofluid flow in the presence of chemical reaction. Conservation equations are solved by applying $SQLM$. The computational results of the suggested technique $(SQLM)$ are compared with those obtained by various researchers ([22],[23], and [24]) under limiting circumstances (see Table 2). For evaluating the Nusselt number, they utilized finite difference scheme, and shooting method (Runge-Kutta-Fehlberg scheme). Gap analysis reveal that the current outcomes are compatible. We investigate the impacts of governing flow parameters on skin-friction coefficient, Nusselt number, and Sherwood number numerically and presented in Table 3. From Table 3, we observed that Skin-friction coefficient enhances consistently together with $Ha, Sc,$ and $Nb,$ whereas it declines consistently upon enhancing δ. Thus, the coefficient of skin-friction coefficient increases with the strength of the Lorentz force. On the other hand, both Nusselt number and Sherwood number decreases with increasing values of Ha and $Nt,$ whereas the buoyancy parameter is to increase both Nusselt and Sherwood number.

5.1. Impacts of Hartman number Ha

An enhancement of the resistance force affiliated with the applied magnetic field generates a drag (force) in terms of Lorentz force, as a result velocity profile and boundary layer thickness declines with an enhancement of the magnetic field. Figure 2 exhibits the influence of the applied magnetic field onto the velocity profile $f'(\eta)$. It has been observed that velocity layout declines with an enhancement of a magnetic parameter, i.e., Hartman number. On the other hand, the resistance affiliated with the Lorentz force by virtue of the applied magnetic field raises the thermal boundary layer, i.e., more heat was generated and raises the thermal boundary layer $\theta(\eta)$ as portrayed in Figure 3.

5.2. Impact of solutal buoyancy parameter δ

Impacts of various values of buoyancy parameter δ on velocity $f'(\eta)$ and temperature $\theta(\eta)$ has been portrayed by Figures 4 and 5 orderly. In a permeable media, fluid velocity is inversely proportional with kinematic viscosity. Again, with an increment in buoyancy parameter viscosity decreases, as a consequence in a permeable media with the increment of buoyancy parameter δ, i.e., with low viscosity fluid velocity $f'(\eta)$ enhanced, which has been portrayed in Figure 4. Whereas from Figure 5 we noticed thermal boundary layer $\theta(\eta)$ are inversely related to buoyancy parameter δ.

5.3. Influence of Prandtl number $\Pr$

The influence of distinct values of the Prandtl number on temperature layout has been portrayed in Figure 6. Prandtl number is a ratio between the momentum diffusivity rate to the heat diffusion rate. It acts as a hyperlink between the fluid stream and the way it impacts the thermal layout. The significance of the Prandtl number is as follows, to identify the dominant terms among momentum and thermal diffusivity, correlative thickness of hydro (fluid) dynamic and thermal boundary layer. An enhancement of viscous force i.e., momentum diffusion and reduction to thermal force, enhance the Prandtl number $\Pr$, consequently, temperature layout diminished as shown in Figure 6.

5.4. Sequel of Brownian motion parameter Nb

Impacts of various values of Brownian motion parameter Nb on temperature layout $\theta(\eta)$ and concentration layout $H(\eta)$ has been exhibited by Figures 7 and 8 orderly. An 'unstable' random movement of particles treated as the Brownian motion. Because of collision, Brownian motion occurs in the fluid during rapid movement of the molecules. An increment on account of random motion of molecules (nano-particles), i.e., an increment in Brownian motion parameter Nb, thermal boundary layer $\theta(\eta)$ is highly effected. The influence of Nb on thermal boundary layer $\theta(\eta)$ is portrayed in Figure 7. Whereas, from Figure 8, we noticed concentration reduces with Brownian parameter.

5.5. Influence of Thermophoresis parameter Nt

Thermophoresis (Thermo migration), is a particular type of force caused by the temperature gradient ΔT affecting the movement from higher to lower temperature walls. An enhancement in the Thermo migration is associated with a rise in the temperature of the fluid. The sequel of this on temperature layout has been displayed in Figure $9.$ In the case of kinematic viscosity diminished i.e., if the buoyancy impact increased, the thermophoretic parametric value will increase which leads to an increment of thermal boundary layer. Thermophoretic and concentration gradients are directly correlated. This physical phenomenon is due to the particle's movement from higher to lower temperature regions. If the heat capacity of the base fluid diminishes or if the heat capacity of the nanoparticles increases, the thermophoresis effect will enhance, as a result, the concentration boundary layer will increase. The concentration outcome due to thermophoretic parameters has been depicted in Figure $10.$

5.6. Influence of Schmidt number Sc

The sequel of rising $Sc,$ Schmidt numbers on the velocity, temperature and concentration layout are depicted in Figures $11,12,$ and 13 respectively. The velocity and the concentration diminished with rising $Sc,$ but Sc and temperature layout are directly related. $Sc,$ represent the ratio of kinematic viscosity (momentum viscosity) and mass diffusivity. With an increase in the value of Schmidt number, kinematic viscosity ν and hence velocity layout of the fluid flow will be diminished. Again, with the increase in the value of the Schmidt number, the mass diffusivity or fluid density or concentration layout will be reduced, consequently, as a consequence thickness of the solutal boundary layer will become thinner. Further, it has been noticed that there will be no indicative influence for enhancing the value of Schmidt number Sc after 2.0 on velocity and temperature layout because of the reduction in the sequel of solutal thermal buoyancy within the flow of fluid.

5.7. Influence of chemical reaction parameter R_1

The influence of chemical reaction parameter R_1 on the temperature and concentration layout are depicted in Figures 14 and 15 respectively. R_1 and temperature layout are directly related (see Figure 14). Whereas, at the time of suction chemical reaction diminishes species of concentration, which is depicted in Figure $15.$

Generation of entropy is affected by multiple pertinent parameters/factors. The alternation in the generation of entropy layout together with numerous valuers of pertinent parameters, for instance, the Brinkman number $Br,$ the Reynolds number $\mathrm{Re},$ and Harmann number Ha were investigated and depicted in several diagrams.

5.8. Entropy generation and Bejan number: Brinkman number

Non-dimensional $Br,$ Brinkman number stated as the fraction of viscous dissipation to thermal conduction in fluid. Brinkman number is a composition of dynamic viscosity $\mu,$ fluid flow velocity, thermal conductivity κ_f, and temperature gradient $\Delta T.$ The impacts of $Br,$ Brinkman number on the generation of entropy $N_G(\eta)$ and Bejan number $Be(\eta)$ has been portrayed in Figures 16 and 17 respectively. From these diagrams it has been noticed that generation of entropy $N_G(\eta)$ and Brinkman number Br are directly related near the stretching sheet, whereas, Brinkman number Br has opposite behaviour with the Bejan number $Be(\eta)$ in the vicinity of the stretching sheet, i.e., with an increment of the $Br,$ Bejan number $Be(\eta)$ declined near the stretching sheet. In the vicinity of the stretching sheet, a significant reduction of heat take place beyond the boundary layer during fluid flow, as a consequence generation of entropy $N_G(\eta)$ rises by enhancing the degree of disorder of the system and declining the Bejan number $Be(\eta).$ Whereas, the impacts of Brinkman number Br is insignificant far from the lamina.

5.9. Entropy generation and Bejan number: Reynolds number

The sequel of Reynolds number Re on the generation of entropy $N_G(\eta)$ depicted in Figure $18.$ In the vicinity of the extended lamina, Reynolds number Re has significant impacts on the generation of entropy $N_G(\eta),$ i.e., with an increment of the Reynolds number Re give rise to a remarkable enhancement in the generation of entropy $N_G(\eta).$ Heat transfer impacts due to diffusion and magnetic field effect caused Reynolds number Re and generation of entropy $N_G(\eta)$ rise together in the neighbourhood of the lamina. Actually, Reynolds number Re is revealed as the quotient of inertia force to viscous force. When forces on account of inertia will be incremented and forces because of viscosity will be reduced, there will be a hike in Reynolds number, as an out – turn fluid acceleration will bump up in the proximity of the sheet. On the other hand, far from the sheet, there are no such ramifications of the Reynolds number $\mathrm{Re}.$

5.10. Entropy generation and Bejan number: Hartmann number

The influence of Hartmann number Ha on the non-dimensional generation of entropy $N_G(\eta)$ and Bejan number $Be(\eta)$ are portrayed in Figures 19 and 20 respectively. In the vicinity of the lamina, remarkable influence of Hartmann number Ha on entropy generation have been noticed, at the same time $Ha,$ Hartmann number has a weak influence on the fluid flow and hence on entropy generation far from the lamina (approx. $\eta \geq 4).$ This impact gives an upwards trend to the motion resistance in the vicinity of the lamina, consequently, the rate of heat transfer increments, yielding a rise in entropy generation number in the neighbourhood of the lamina. However, far away from the sheet, the impact of $Ha,$ Hartmann number is just contrary, irreversibility due to entropy has a slow decreasing tendency with the increasing value of Ha and declining the Bejan number $Be(\eta)$ (see Figure 20).

6. Conclusion

The current investigation has been manifested to examine the generation of entropy of MHD viscoelastic nanofluids stream together with chemical reaction. Graphical representations were acquired to exhibit the notable influence of some non-dimensional pertinent parameters on generation of entropy as well as on Bejan number together with velocity, thermal boundary layer and concentration layouts. We deduce as follows from present perusal:

- Thermal $\theta(\eta)$ and Brownian motion parameter Nb are directly associated, while, concentration $H(\eta)$, as well as velocity layout $f'(\eta)$, are reverse in nature with Nb.
- An increment in the Thermo migration Nt is associated with a rise in temperature, concentration and fluid velocity.
- The velocity and the concentration diminished with rising Sc, but Sc and temperature layout are directly related.
- Physically chemical reaction parameter R_1 minimizes the momentum diffusivity and mass transportation whereas the heat transportation rises.
- In the vicinity of the extended lamina, Br and entropy generation are related directly in spite of that an opposite behaviour for the Bejan number Be has been observed.

References

1 Tlili, I., Shahmir, N., Ramzan, M., et al. "A novel model to analyze Darcy Forchheimer nanofluid flow in a permeable medium with Entropy generation analysis", *J. Taibah Univ. Sci.*, ***14***(1), pp. 916-930 (2020). DOI: https://doi.org/10.1080/16583655.2020.1790171

2 Khan, M.N. and Nadeem, S. "Theoretical treatment of bio-convective Maxwell nanofluid over an exponentially stretching sheet", *Can. J. Phys.*, ***98***(8), pp. 732-741 (2020). DOI: https://doi.org/10.1139/cjp-2019-0380

3 Ramzan, M., Shahmir, N., and Ghazwani, H.A.S. "Mixed convective Casson partially ionized nanofluid flow amidst two inclined concentric cylinders with gyrotactic microorganisms", *Waves Random Complex Media*, pp. 1-21 (2022). DOI: https://doi.org/10.1080/17455030.2022.2110623

4 Nadeem, S., Khan, M.N., Muhammad, N., et al. "Mathematical analysis of bio-convective micropolar nanofluid", *J. Comput. Des. Eng.*, ***6***(3), pp. 233-242 (2019). DOI: https://doi.org/10.1016/j.jcde.2019.04.001

5 Mondal, H., Mandal, A., and Tripathi, R. "Numerical investigation of the non-Newtonian power-law fluid with convective boundary conditions in a non-Darcy porous medium", *Waves Random Complex Media*, pp. 1-17 (2022). DOI: https://doi.org/10.1080/17455030.2022.2123966

6 Khan, M.N., Nadeem, S., and Muhammad, N. "Micropolar fluid flow with temperature-dependent transport properties", *Heat Transfer*, ***49***(4), pp. 2375-2389 (2020). DOI: https://doi.org/10.1002/htj.21726

7 Ahmad, S., Nadeem, S., Muhammad, N., et al. "Cattaneo–Christov heat flux model for stagnation point flow of micropolar nanofluid toward a nonlinear stretching surface with slip effects", *J. Therm. Anal. Calorim.*, ***143***, pp. 1187-1199 (2021). DOI: https://doi.org/10.1007/s10973-020-09504-2

8 Khan, M.N., Ullah, N., and Nadeem, S. "Transient flow of Maxwell nanofluid over a shrinking surface: Numerical solutions and stability analysis", *Surf. Interfaces*, ***22***, pp. 100829 (2021). DOI: https://doi.org/10.1016/j.surfin.2020.100829

9 Ramzan, M., Ali, J., Shahmir, N., et al. "Thermophoretic particle deposition impact in the Oldroyd-B fluid flow influenced by a magnetic dipole with an exponential thermal heat source", *Int. J. Mod. Phys. B*, ***37***(06), pp. 2350059 (2023). DOI: https://doi.org/10.1142/S0217979223500595

10 Kumar, A., Ray, R.K., and Sheremet, M.A. "Entropy generation on double-diffusive MHD slip

flow of nanofluid over a rotating disk with nonlinear mixed convection and Arrhenius activation energy", *Indian J. Phys.*, pp. 1-17 (2022). DOI: https://doi.org/10.1007/s12648-021-02015-2

11 Ahmad, S., Khan, M.N., and Nadeem, S. "Mathematical analysis of heat and mass transfer in a Maxwell fluid with double stratification", *Phys. Scr.*, ***96***(2), pp. 025202 (2020). DOI: https://doi.org/10.1088/1402-4896/abcb2a

12 Krishna, M.V., & Chamkha, A.J. "Hall and ion slip impacts on unsteady MHD convective flow of Ag-TiO2/WEG hybrid nanofluid in a rotating frame", *Curr. Nanosci.*, ***19***(1), pp. 15-32 (2023). DOI: https://doi.org/10.2174/1573413717666211018113823

13 Khan, U., Zaib, A., and Mebarek-Oudina, F. "Mixed convective magneto flow of SiO 2–MoS 2/C 2 H 6 O 2 hybrid nanoliquids through a vertical stretching/shrinking wedge: Stability analysis", *Arabian J. Sci. Eng.*, ***45***, pp. 9061-9073 (2020). DOI: https://doi.org/10.1007/s13369-020-04680-7

14 Vaidya, H., Rajashekhar, C., Mebarek-Oudina, F., et al. "Examination of chemical reaction on three dimensional mixed convective magnetohydrodynamic Jeffrey nanofluid over a stretching sheet", *Journal of Nanofluids*, ***11***(1), pp. 113-124 (2022). DOI: https://doi.org/10.1166/jon.2022.1817

15 Ramzan, M., Shaheen, N., Ghazwani, H. A. S., et al. "Application of Corcione correlation in a nanofluid flow on a bidirectional stretching surface with Cattaneo–Christov heat flux and heat generation/absorption", *Numerical Heat Transfer, Part A: Applications*, ***84***(6), pp. 569-585 (2022). DOI: https://doi.org/10.1080/10407782.2022.2145396

16 Khan, M. N., Nadeem, S., Ullah, N., and Saleem, A. "Theoretical treatment of radiative Oldroyd-B nanofluid with microorganism pass an exponentially stretching sheet", *Surf. Interfaces*, ***21***, pp. 100686 (2020). DOI: https://doi.org/10.1016/j.surfin.2020.100686

17 Pal, D., Das, B. C., and Vajravelu, K. "Magneto-Soret-Dufour thermo-radiative double-diffusive convection heat and mass transfer of a micropolar fluid in a porous medium with Ohmic dissipation and variable thermal conductivity", *Propul. Power Res.*, ***11***(1), pp. 154-170 (2022). DOI: https://doi.org/10.1016/j.jppr.2022.02.001

18 Rafiq, M., Sajid, M., Alhazmi, S. E., et al. "MHD electroosmotic peristaltic flow of Jeffrey nanofluid with slip conditions and chemical reaction", *Alexandria Eng. J.*, ***61***(12), pp. 9977-9992 (2022). DOI: https://doi.org/10.1016/j.aej.2022.03.035

19 Reddy, N. N., Reddy, Y. D., Rao, V. S., et al. "Multiple slip effects on steady MHD flow past a non-isothermal stretching surface in presence of Soret, Dufour with suction/injection", *Int. Commun. Heat Mass Transfer*, ***134***, pp. 106024 (2022). DOI: https://doi.org/10.1016/j.icheatmasstransfer.2022.106024

20 Gul, T., Khan, A., Bilal, M., et al. "Magnetic dipole impact on the hybrid nanofluid flow over an extending surface", *Sci. Rep.*, ***10***(1), pp. 8474 (2020). DOI: https://doi.org/10.1038/s41598-020-65298-1

21 Sarkar, A., Mondal, H., and Nandkeolyar, R. "Powell-Eyring Fluid Flow Over a Stretching Surface with Variable Properties", *Journal of Nanofluids*, ***12*(**1), pp. 47-54 (2023). DOI: https://doi.org/10.1166/jon.2023.1908

22 Chen, C. H. "Laminar mixed convection adjacent to vertical, continuously stretching sheets", *Heat Mass transfer*, ***33***, pp. 471-476 (1998). DOI: https://doi.org/10.1007/s002310050217

23 Ishak, A., Nazar, R., and Pop, I. "Hydromagnetic flow and heat transfer adjacent to a stretching vertical sheet", *Heat Mass Transfer*, ***44***(8), pp. 921-927 (2008). DOI: https://doi.org/10.1007/s00231-007-0322-z

24 Pal, D. and Mondal, H. "Soret and Dufour effects on MHD non-Darcian mixed convection heat and mass transfer over a stretching sheet with non-uniform heat source/sink", *Physica B*, ***407***(4), pp. 642-651 (2012). DOI: https://doi.org/10.1016/j.physb.2011.11.051

25 Bhukta, D., Dash, G. C., Mishra, S. R., et al. "Dissipation effect on MHD mixed convection flow over a stretching sheet through porous medium with non-uniform heat source/sink", *Ain Shams*

Eng. J., ***8***(3), pp. 353-361 (2017). DOI: https://doi.org/10.1016/j.asej.2015.08.017
26 Mondal, H., Pal, D., Chatterjee, S., et al. "Thermophoresis and Soret-Dufour on MHD mixed convection mass transfer over an inclined plate with non-uniform heat source/sink and chemical reaction", *Ain Shams Eng. J.*, ***9***(4), pp. 2111-2121 (2018). DOI: https://doi.org/10.1016/j.asej.2016.10.015
27 Wang, F., Khan, S. A., Gouadria, S., et al. "Entropy optimized flow of Darcy-Forchheimer viscous fluid with cubic autocatalysis chemical reactions", *Int. J. Hydrogen Energy*, ***47***(29), pp. 13911-13920 (2022). DOI: https://doi.org/10.1016/j.ijhydene.2022.02.141

Author Biography

- **Arindam Sarkar** is a PhD Scholar at the National Institute of Technology Jamshedpur, Jamshedpur, India under the supervision of Dr. Raj Nandkeolyar and Dr. Hiranmoy Mondal. His field of research is fluid dynamics. Currently working on the hybrid nanofluid model. His research work is focused on the following areas: Newtonian, non-Newtonian fluids, MHD, heat transfer, mass transfer, nanofluids, hybrid nanofluids, spectral quasi linearization method (SQLM).

- **Dr. Hiranmoy Mondal** received the M.Sc. degrees in Mathematics and Computing from Indian Institute of Technology (Indian School of Mines) Dhanbad and awarded Ph.D. degree in Mathematics from Visva-Bharati University, Santiniketan. He received Claude Leon Foundation Postdoctoral Research Fellowship from University of KwaZulu Natal, South Africa in 2016–2018. Presently, he is serving as an Associate Professor and Head of the Department of Applied Mathematics, Maulana Abul Kalam Azad University of Technology, India. Besides teaching he is actively engaged in research in the field of Fluid mechanics particularly, in boundary layer flows, Newtonian/non-Newtonian fluids, heat and mass transfer in porous/non-porous media and different types of nanofluids.

- **Dr. Raj Nandkeolyar** received his Ph. D. degree in Applied Mathematics with specialization in fluid mechanics from Indian Institute of Technology (Indian School of Mines) Dhanbad, Dhanbad, India in the year 2011. He was a Post – doctoral fellow in the School of Mathematics, Statistics & Computer Sciences, University of KwaZulu- Natal, Pietermaritzburg, South Africa. Presently, he is serving as an Associate Professor in the Department of Mathematics, National Institute of Technology Jamshedpur, Jamshedpur, India. His research interests include modelling the fluid flow problems involving Newtonian and non-Newtonian fluids, heat transfer, mass transfer and the application of spectral methods on these problems.

7. Appendices sections:

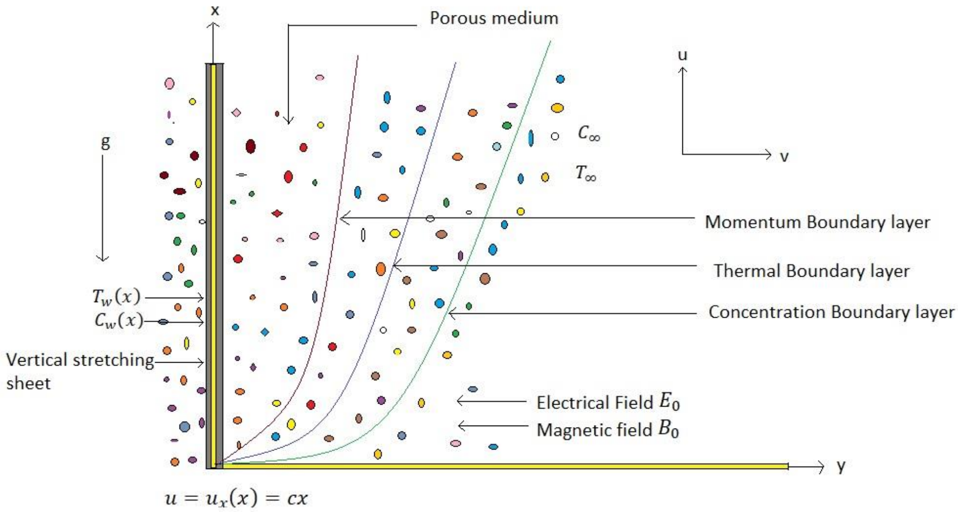

Figure 1. Physical model and Co-ordinate system

Table 1. Gap Analysis		
Authors	Considered problem	Findings
Chen [22]	Effects of velocity and temperature on power law fluid with buoyancy force, utilized the finite difference method.	Heat transfer depends on buoyancy parameter, Prandtl number, velocity, and temperature exponent parameter.
Ishak, Nazar, and Pop. [23]	Effects of velocity and temperature on electrically conducting MHD power law fluid, solved by Keller – box method.	Skin-friction and Nusselt number decline as magnetic parameter enhances.
Pal and Mondal [24]	Impacts of non-constant heat source/sink on electrically conducting incompressible fluid, utilized Runge-Kutta-Fehlberg Fifth order method.	Impacts of the coefficients of the skin-friction, heat transfer coefficient, and local Sherwood number also has been determined numerically.
Bhukta et al. [25]	Dissipative effect on electrically conducting unsteady flow in a porous medium, solved by Runge-Kutta fourth order method.	Skin-friction reduces with Prandtl number, but positively related with electric field.
Mondal et al. [26]	Semi-infinite permeable inclined flat plate in the presence of chemical reaction, used Runge-Kutta-Fehlberg Fifth order method.	As the angle of inclination increases, thermal and concentration layout enhances, but velocity layout decreases.
Wang et al. [27]	Darcy-Forchheimer viscous fluid with chemical reactions, utilized ND-solve procedure.	Thermal layout enhances with heat generation parameter, reduces with thermal slip parameters.

Table 2. Comparison of $-\theta'(0)$ for different values of $\Pr, Nt \to 0, Nb \to 0$ and the remaining parameters are zero.

Pr	Chen [22]	Ishak et al. [23]	Pal and Mondal [24]	Our Outcomes
1.0	1.33334	1.3333	1.333333	1.33333333
2.0	–	–	2.000000	1.99999557
3.0	2.50997	2.5097	2.509725	2.50972157
5.0	–	–	3.316482	3.31647940
10.0	4.79686	4.7969	4.796873	4.79687060

Table 3. The values of coefficient of skin-friction, local Nusselt number, local Sherwood number for various parameters

Ha	δ	Sc	Nb	Nt	$C_f \mathrm{Re}_x^{\frac{1}{2}}$	$\mathrm{Re}_x^{-\frac{1}{2}} Nu_x$	$\mathrm{Re}_x^{-\frac{1}{2}} Sh_x$
0.1	0.4	0.22	0.5	0.4	0.97253011	1.20882119	–0.03420891
0.5					1.07530119	1.19042791	–0.04151450
1.0					1.35814201	1.13811685	–0.05680289
	0.4				1.12123485	1.92980389	–0.66162882
	0.7				0.92423144	1.94490734	–0.61169790
	1.0				0.73877730	1.96051643	–0.57613154
		0.22			0.87365049	1.65942751	–0.59663825
		0.50			0.92014739	1.39188005	0.17182333
		0.66			0.93510072	1.30278878	0.47385202
			0.5		0.84929188	1.77529010	–1.23105777
			0.7		0.87365049	1.65942751	–0.59663825
			0.9		0.88703996	1.55379907	–0.25039234
				0.2	1.09572872	1.88814549	0.24995326
				0.4	1.07534106	1.77834780	–0.21879220
				0.6	1.05671776	1.67772325	–0.61490050

Nomenclature

a,b,c,D	constants	Re	Reynolds number
A^*,B^*	coefficient of space and temperature-dependent heat source/sink	Sc	Schmidt number
B_0	magnetic field strength	Sh	Sherwood number
Br	Brinkman number	T	temperature $[K]$
C	concentration of the species	T_w	wall temperature of the lamina
C_w	concentration at the surface	T_∞	ambient temperature
C_∞	ambient concentration	ΔC	difference between $(C_w - C_\infty)$
c_b	coefficient of drag force	ΔT	difference between $(T_w - T_\infty)$
C_f	coefficient of skin friction	x, y	Cartesian coordinates $[m]$
c_p	specific heat $\left[Jkg^{-1}K^{-1}\right]$	u,v	velocities along x and y directions $\left[ms^{-1}\right]$
D_B	diffusion coefficient of species	u_w	velocity of the stretching sheet
D_T	thermophoretic diffusion coefficient	**Greek symbols**	
E_c	Eckert number	$\sum$	dimensionless parameter
E_0	electric strength $[V/m]$	β_T	thermal expansion coefficient
E_1	electric parameter	ν	kinematic viscosity $\left[m^2s^{-1}\right]$
f	dimensionless velocity	β_C	concentration expansion coefficient
F^*	inertia coefficient	δ	concentration buoyancy parameter
g	gravitational acceleration $\left[ms^{-2}\right]$	ρ	fluid density $\left[kgm^{-3}\right]$
Gr_x	local Grashof number	η	dimensionless variable
Gr_c	solutal Grashof number	μ	dynamic viscosity $\left[kgm^{-1}s^{-1}\right]$
H	Dimensionless concentration	κ_f	thermal conductivity $\left[Wm^{-1}K^{-1}\right]$
k_1	porosity parameter	τ	fraction of heat capacity of nanoparticles to the base fluid
Ha	Hartmann number	ψ	stream function of the fluid
R_1	chemical reaction parameter	θ_w	temperature ratio parameter
κ	permeability $\left[m^2\right]$	σ	electrical conductivity $\left[Sm^{-1}\right]$
Nb	Brownian motion parameter	λ	thermal buoyancy parameter
Nt	thermophoresis parameter	θ	dimensionless temperature
Nu	Nusselt number	χ,Ω	constant parameters
Pr	Prandtl number $\left[\frac{mol}{L.s}\right]$		
q'''	Non-uniform heat source/sink		

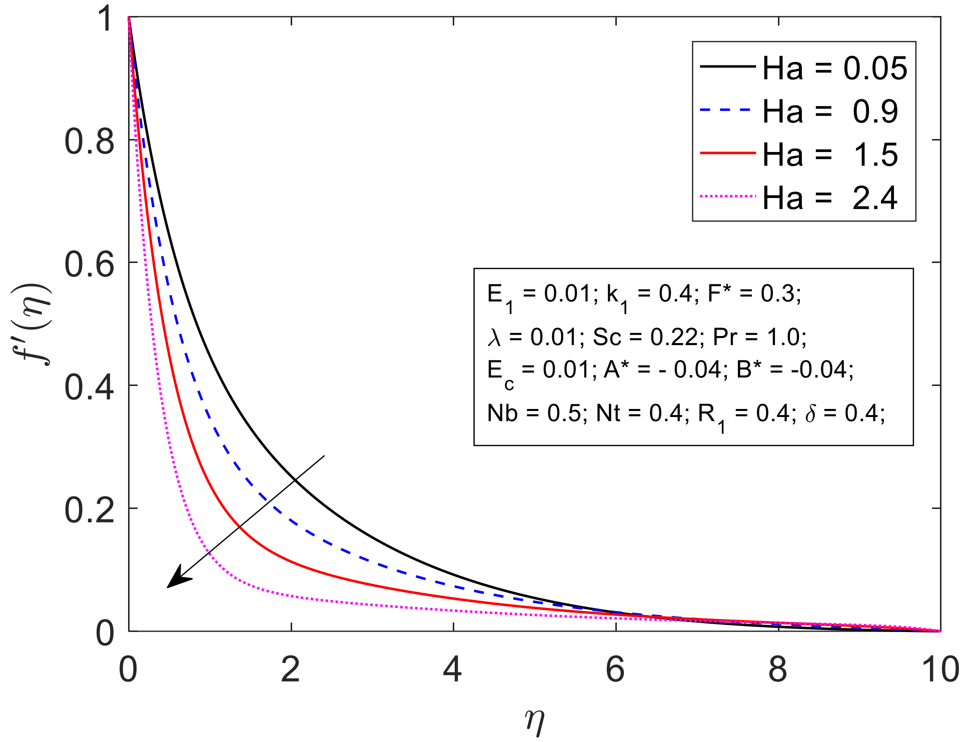

Figure 2. Impact of Ha on $f'(\eta)$

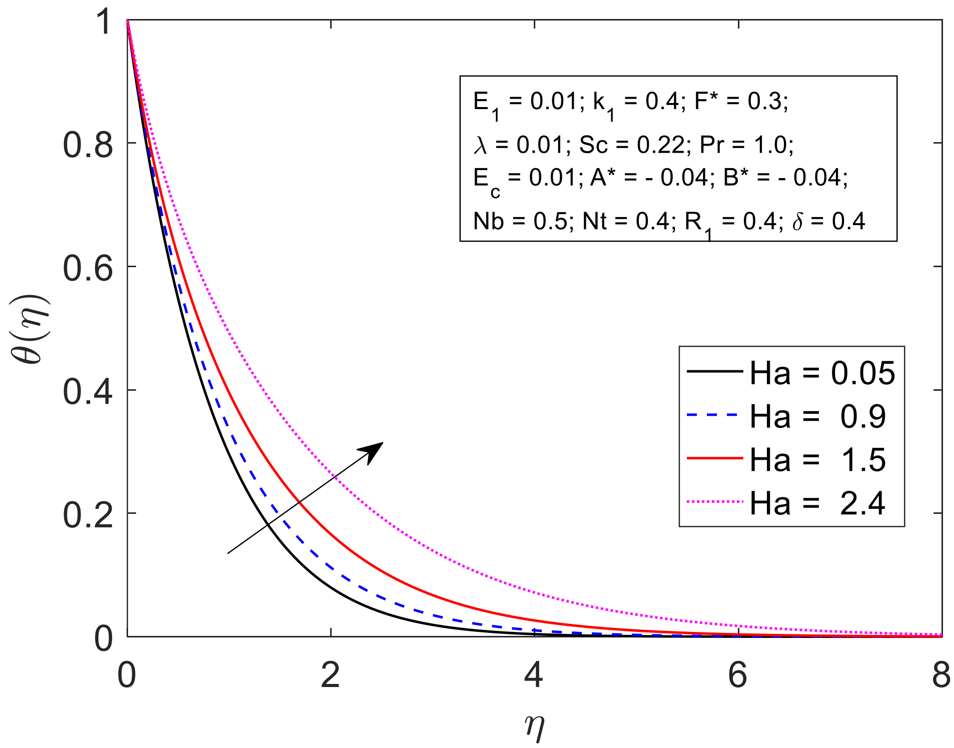

Figure 3. Impact of Ha on $\theta(\eta)$

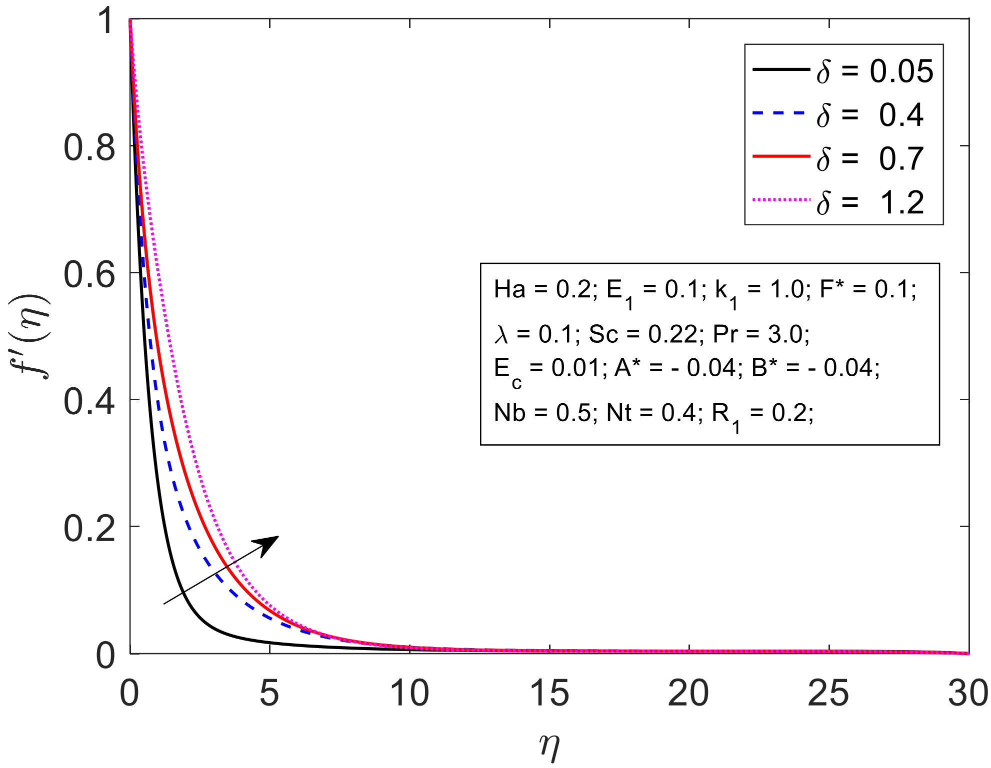

Figure 4. Impact of δ on $f'(\eta)$

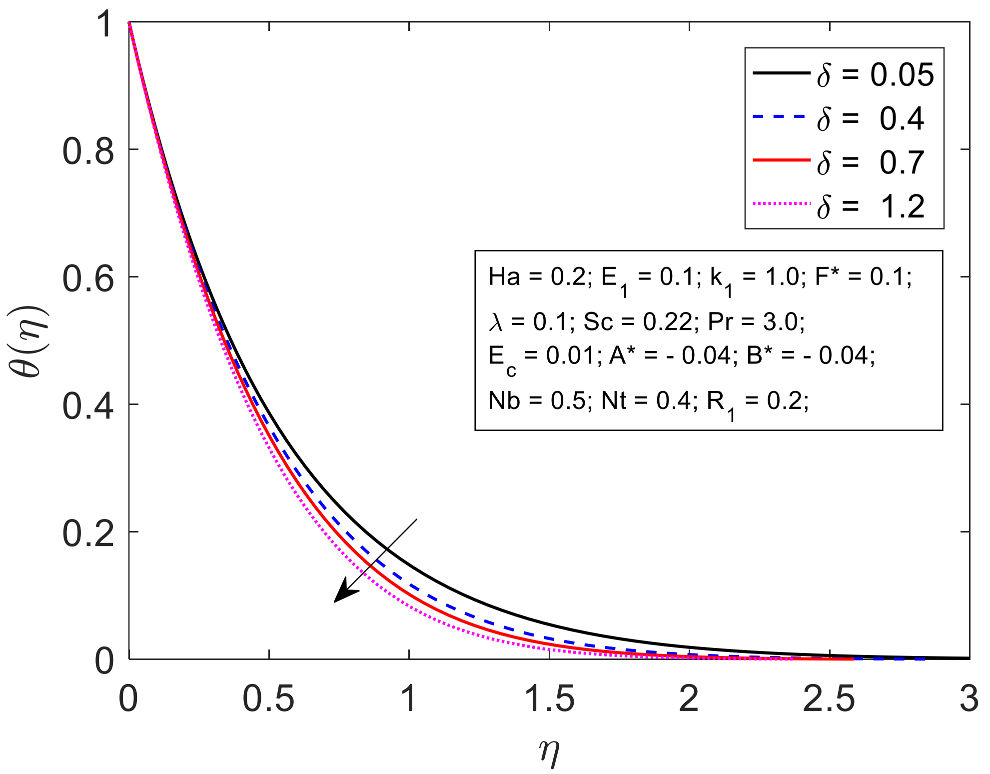

Figure 5. Impact of δ on $\theta(\eta)$

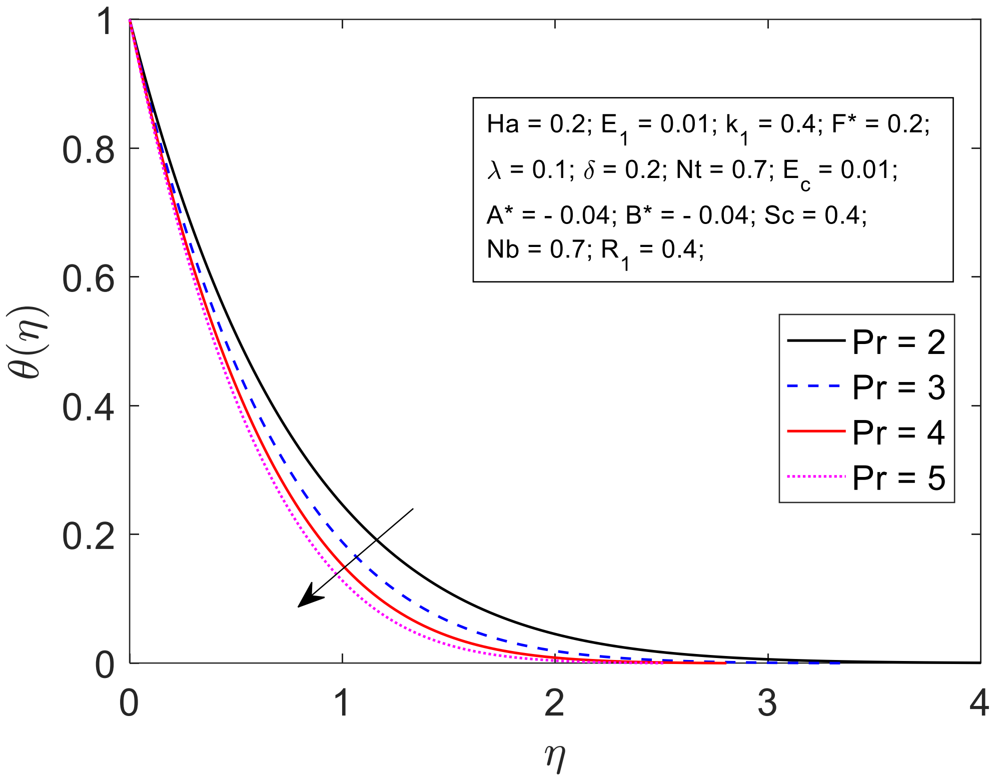

Figure 6. Impact of $\Pr$ on $\theta(\eta)$

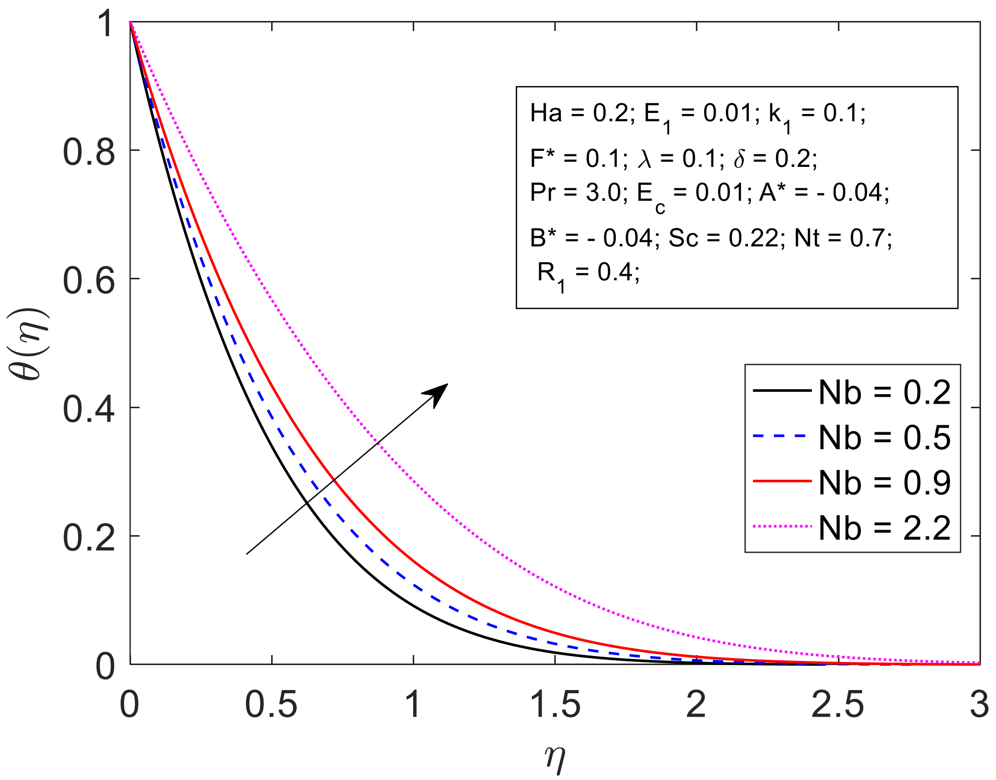

Figure 7. Impact of Nb on $\theta(\eta)$

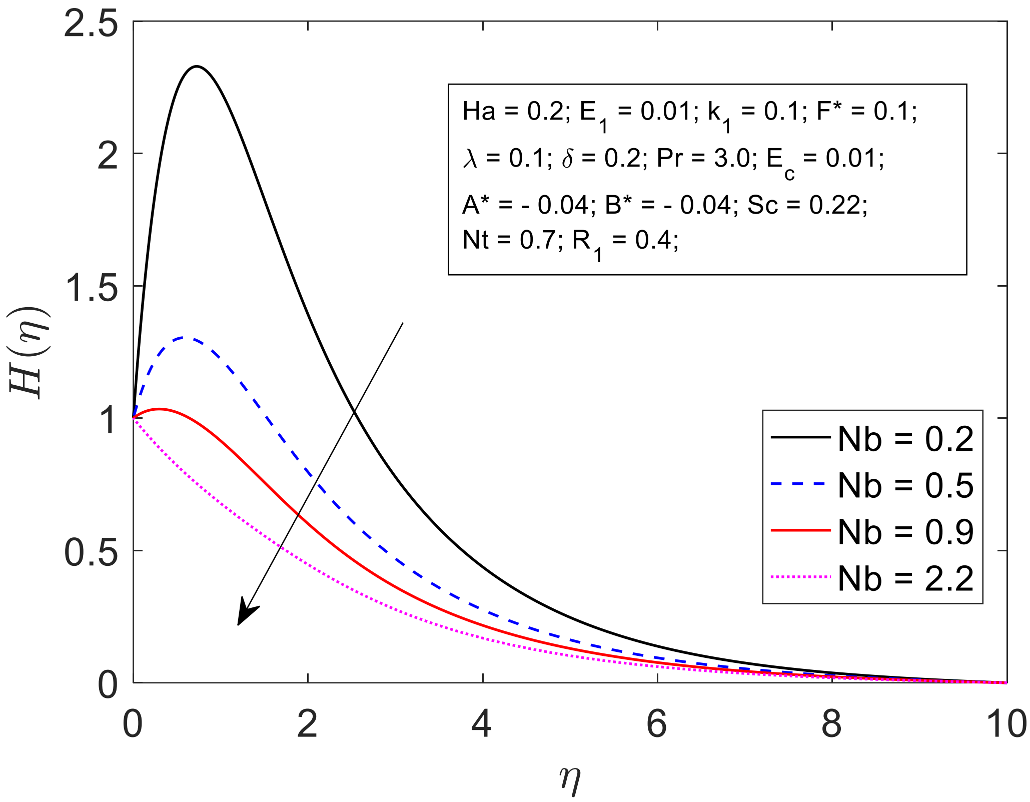

Figure 8. Impact of Nb on $H(\eta)$

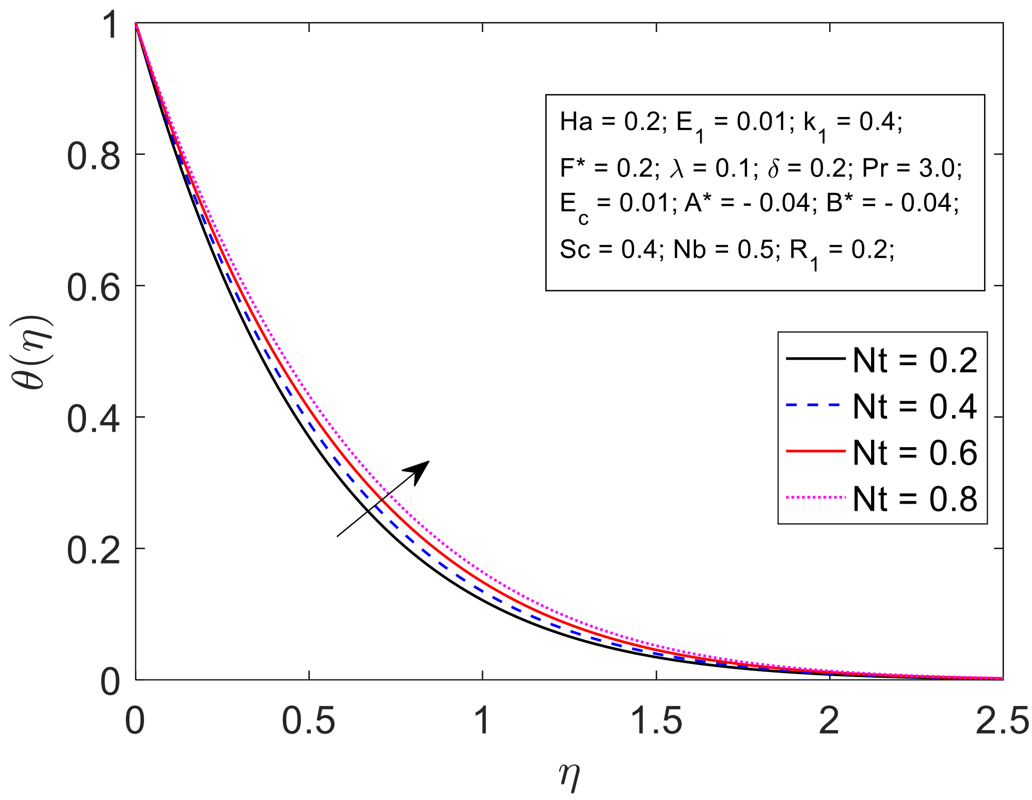

Figure 9. Impact of Nt on $\theta(\eta)$

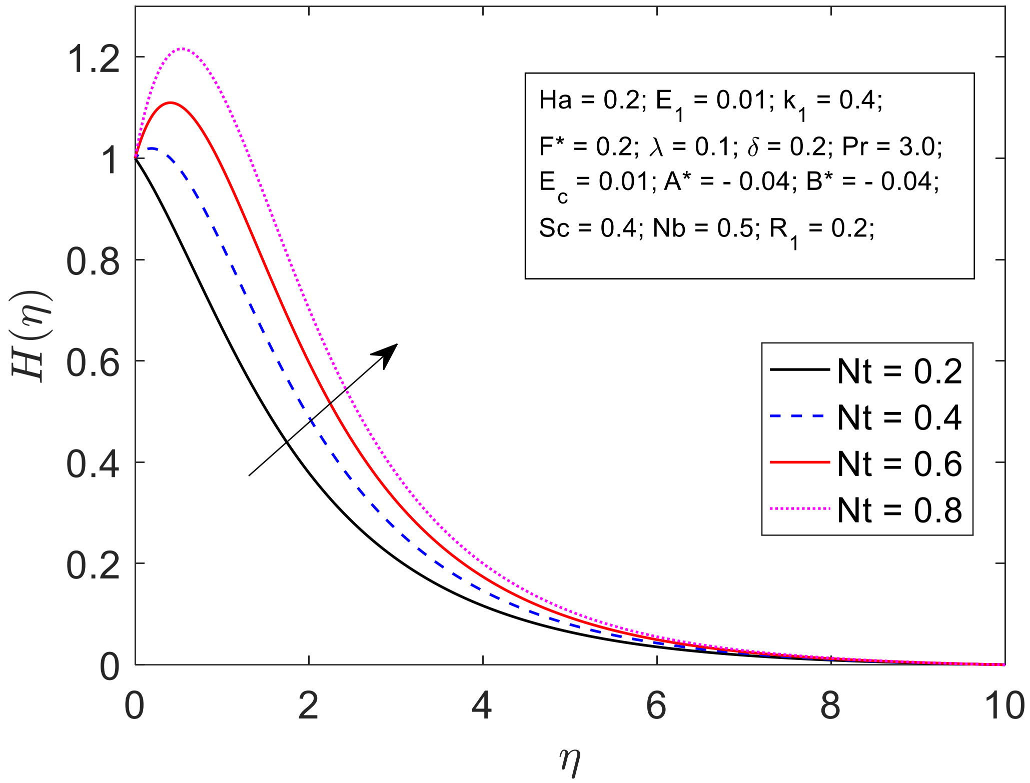

Figure 10. Impact of Nt on $H(\eta)$

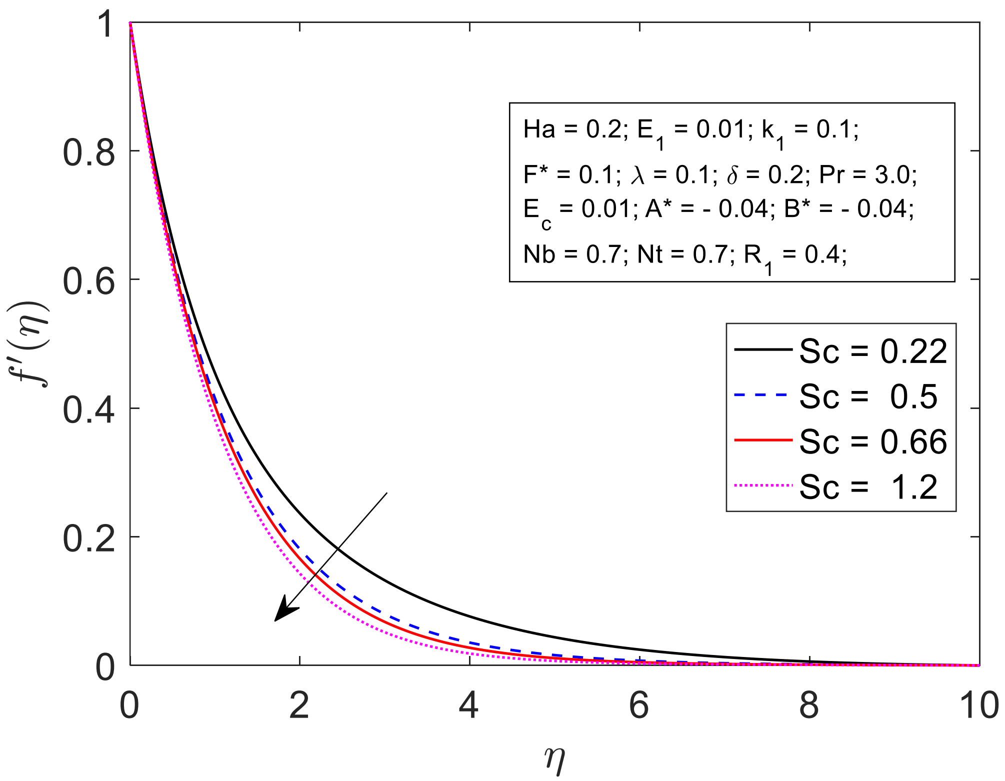

Figure 11. Impact of Sc on $f'(\eta)$

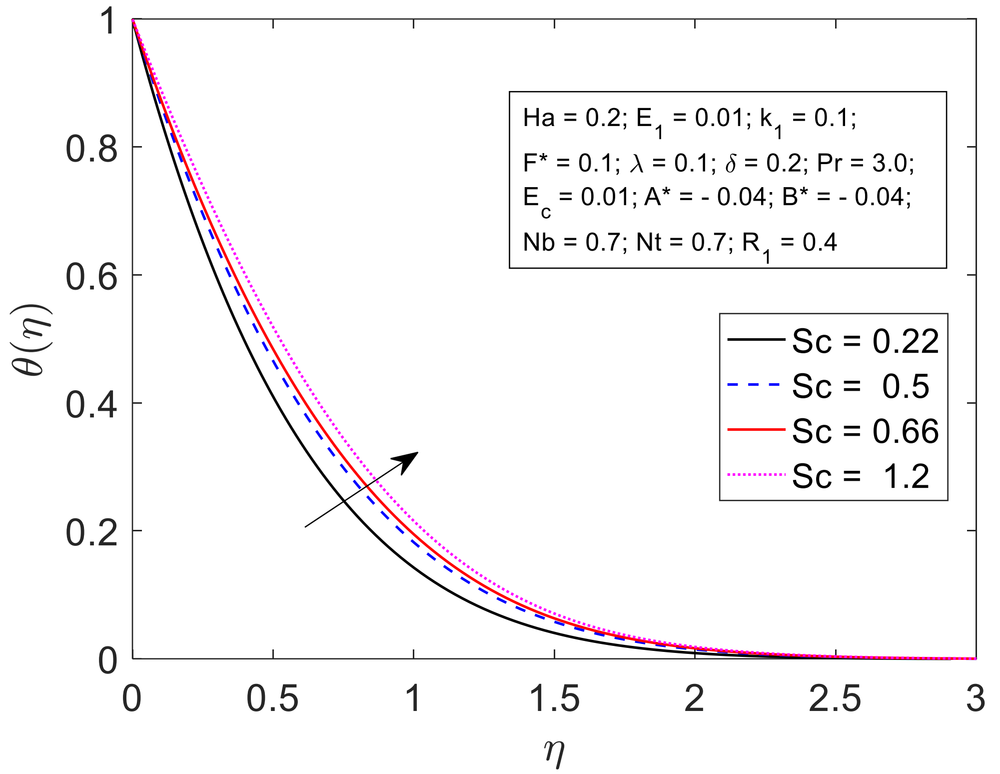

Figure 12. Impact of Sc on $\theta(\eta)$

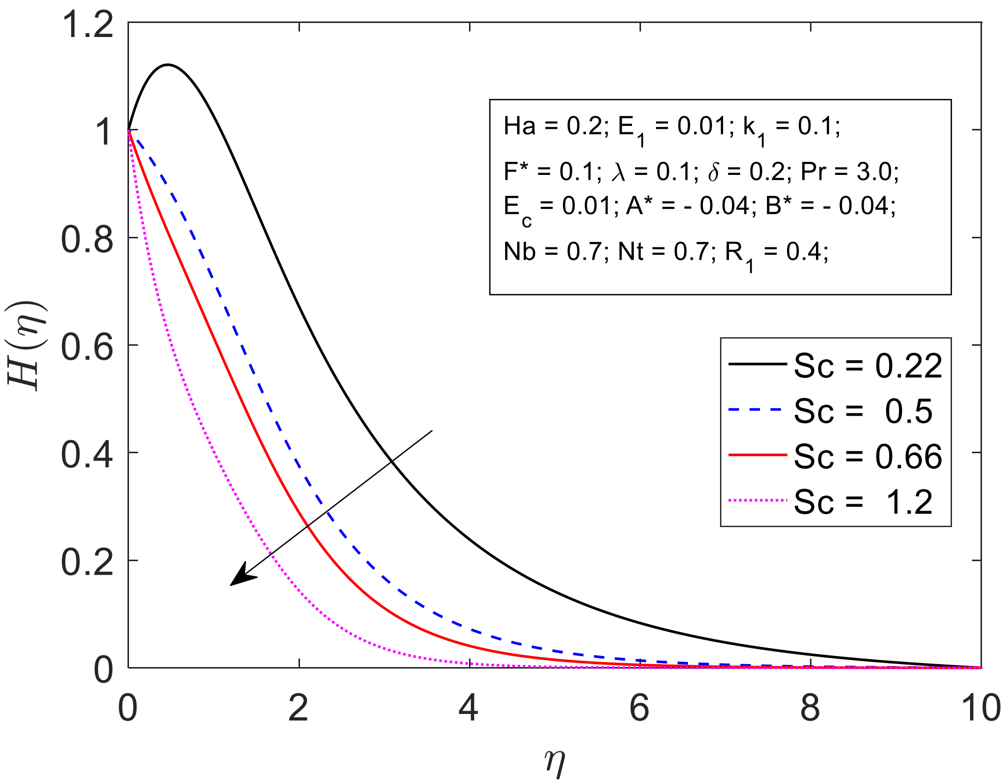

Figure 13. Impact of Sc on $H(\eta)$

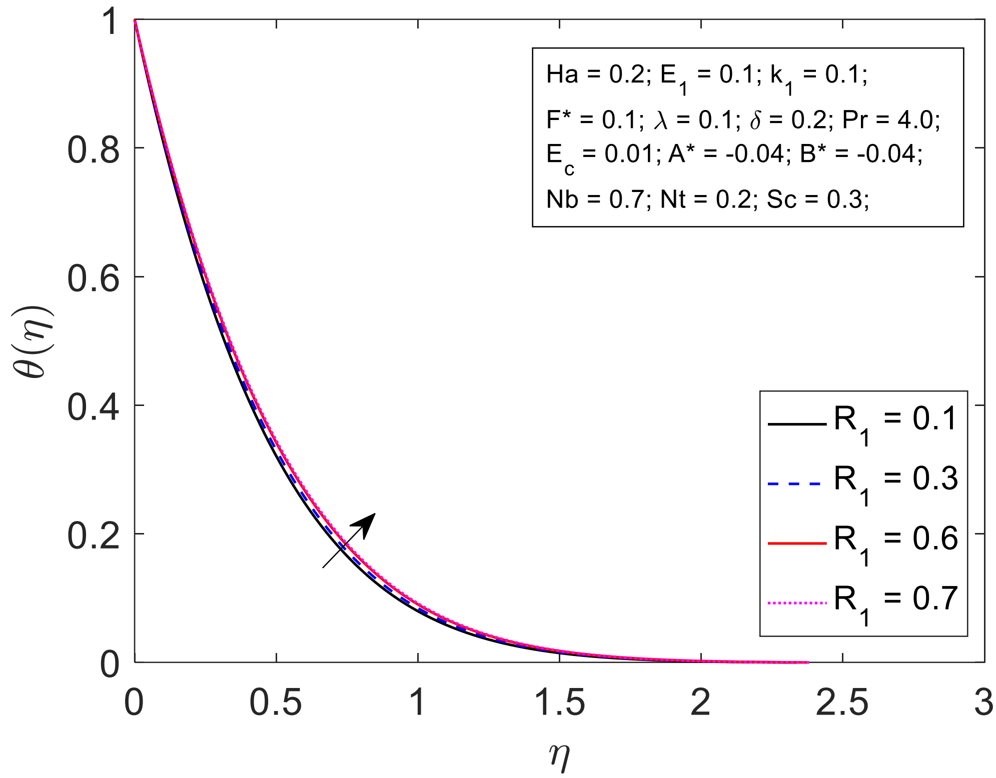

Figure 14. Impact of R_1 on $\theta(\eta)$

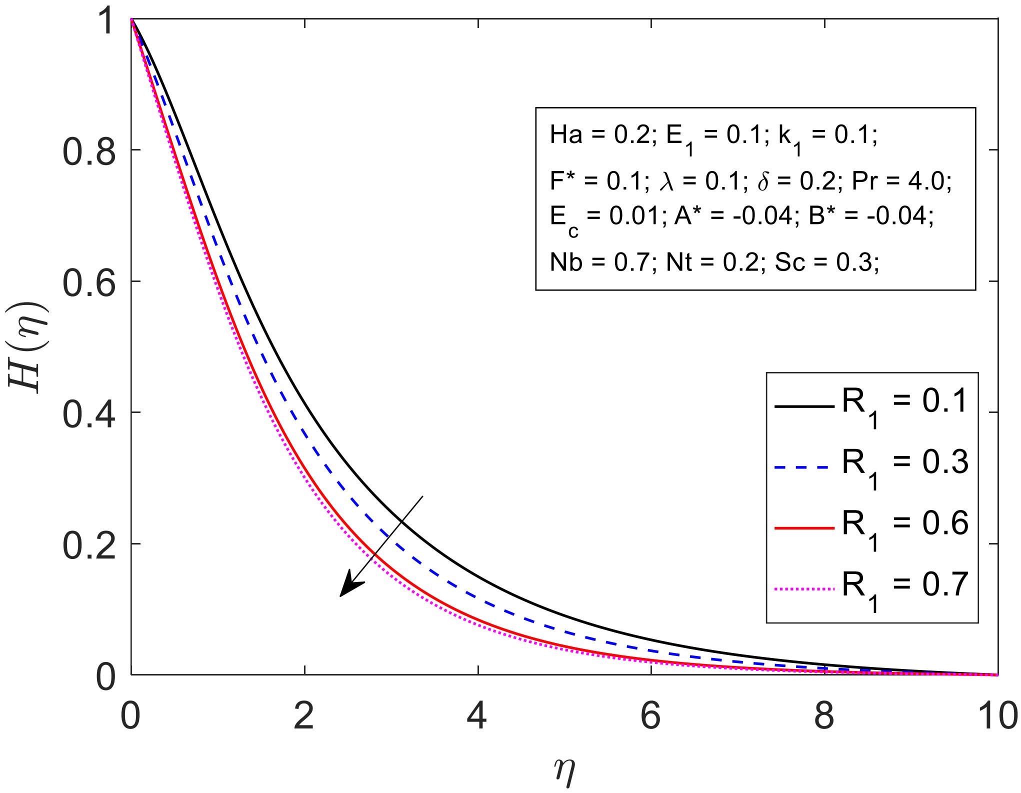

Figure 15. Impact of R_1 on $H(\eta)$

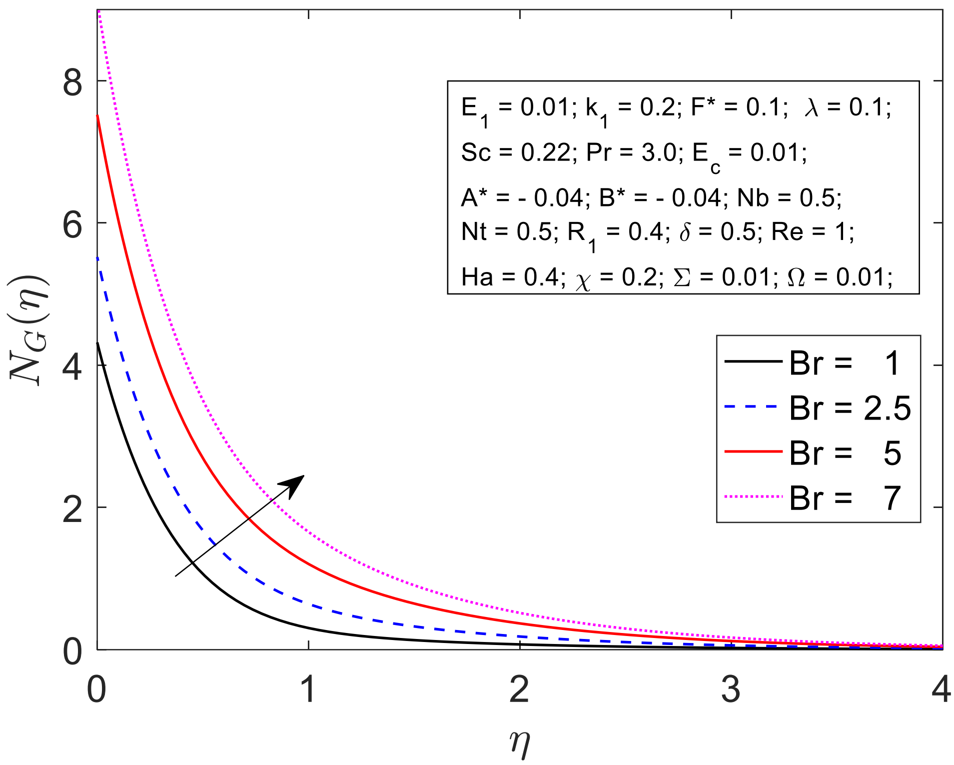

Figure 16. Impact of Br on $N_G(\eta)$

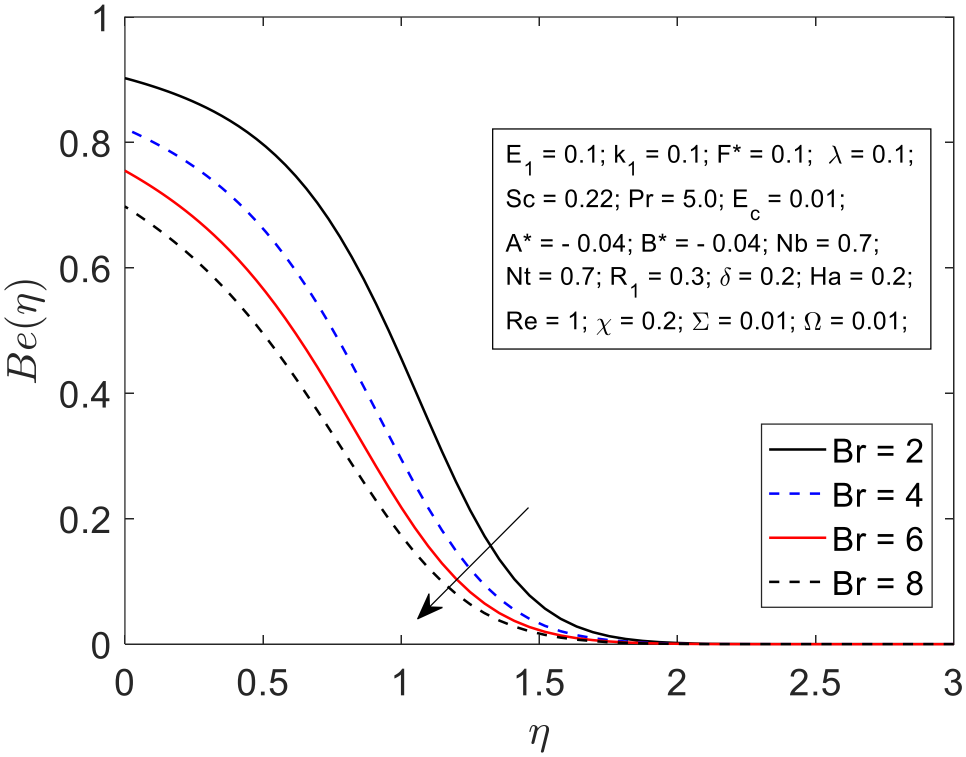

Figure 17. Impact of Br on $Be(\eta)$

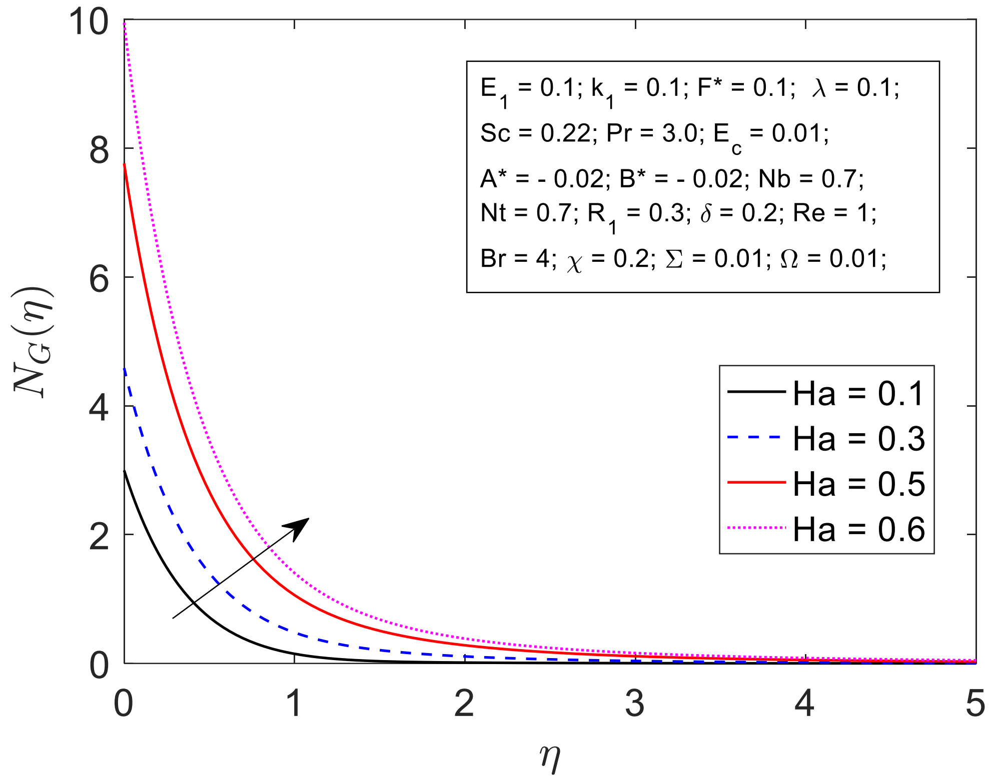

Figure 18. Impact of Ha on $N_G(\eta)$

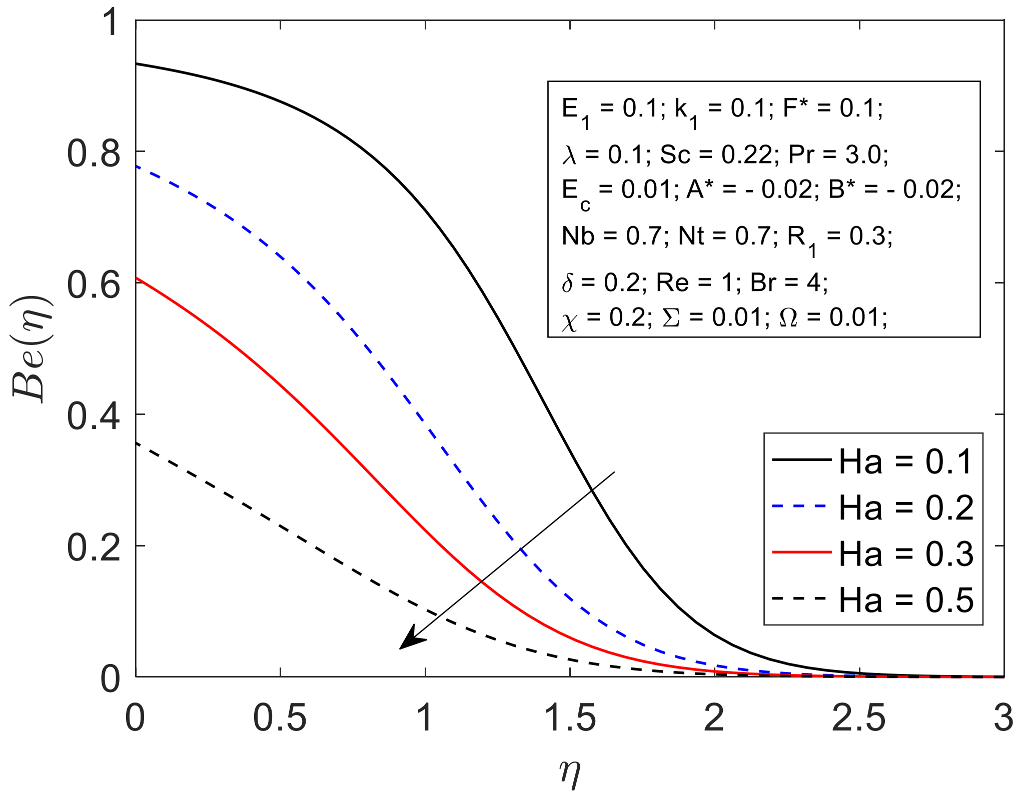

Figure 19. Impact of Ha on $Be(\eta)$

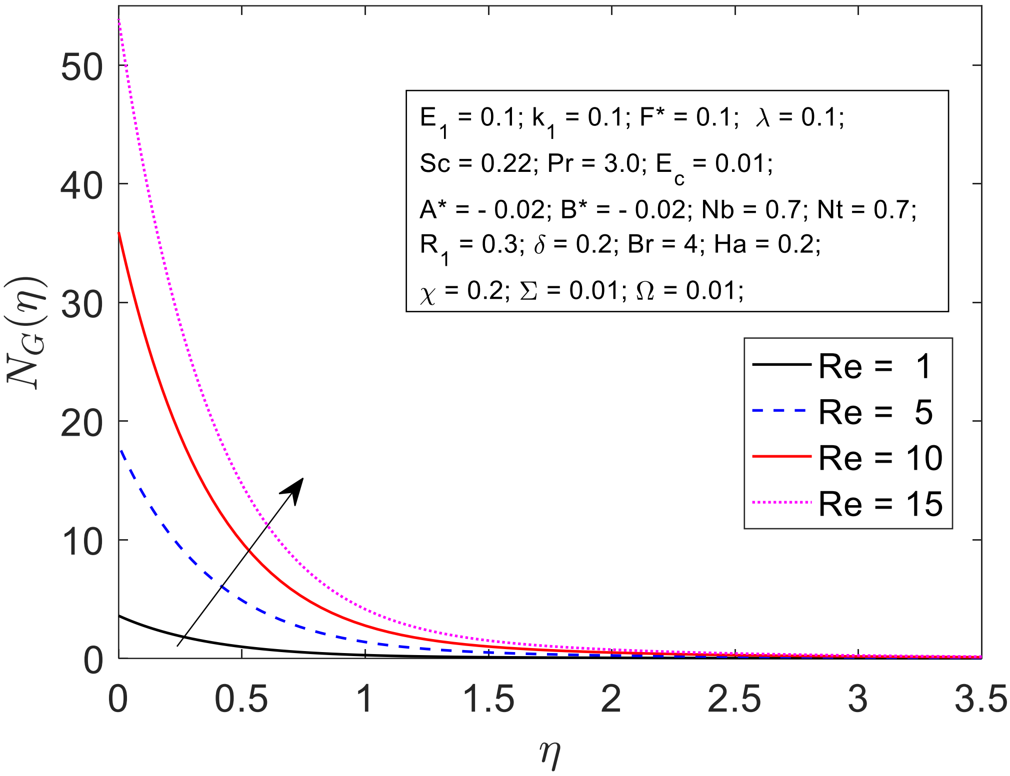

Figure 20. Impact of Re on $N_G(\eta)$